ORNL/TM-2022/2544

Gray-Box Fault Models and Applications for Low–Carbon Emission CO_2 Refrigeration Systems

Yanfei Li
Jian Sun
Brian Fricke
Piljae Im
Teja Kuruganti

July 2022

OAK RIDGE National Laboratory

ORNL IS MANAGED BY UT-BATTELLE LLC FOR THE US DEPARTMENT OF ENERGY

ORNL/TM-2022/2544

Electrification and Energy Infrastructures Division

GRAY-BOX FAULT MODELS AND APPLICATIONS FOR LOW–CARBON EMISSION CO_2 REFRIGERATION SYSTEMS

Yanfei Li
Jian Sun
Brian Fricke
Piljae Im
Teja Kuruganti

July 2022

Prepared by
OAK RIDGE NATIONAL LABORATORY
Oak Ridge, TN 37831
managed by
UT-BATTELLE LLC
for the
US DEPARTMENT OF ENERGY
under contract DE-AC05-00OR22725

CONTENTS

LIST OF FIGURES

EXECUTIVE SUMMARY

Carbon dioxide refrigeration systems have attracted increased attention in recent years because of their zero-carbon emission advantages compared with traditional refrigerants. These systems are widely used in certain commercial buildings such as supermarkets. However, few energy studies have been conducted for such refrigeration systems under fault conditions. This study investigated five common faults for supermarket transcritical CO_2 refrigeration systems with display cases. The following major tasks were implemented for this study. First, five fault models (gray-box format) regarding the power consumption and supply air temperature were proposed for both low- and high-temperature display cases. The models cover ice accumulation on the evaporator coil, evaporator fan partial failure, expansion valve failure, display door open, and condenser blockage. Next, the fault models were calibrated with field tests, and the modeling accuracies were in good agreement with measurement data sets. Finally, the proposed fault models demonstrated more than 90% of fault detection for fault detection and diagnostics purposes for both field measurements and simulations.

1. INTRODUCTION

1.1 BACKGROUND

In the United States, the building sector accounts for 40% of the total energy consumption and 75% of power demands (Sofos et al. 2020). The power demands mainly come from HVAC system use to maintain the desired indoor temperature and humidity. Supermarkets are a commercial building type with intense energy consumption. According to the Food Marketing Institute ("Supermarket Facts" 2021), as of 2018, approximately 38,000 supermarkets exist in the United States, and the median floor area is around 46,000 ft^2 (4,300 m^2). For supermarkets, approximately 50% of the electrical energy is consumed by refrigeration systems. Another study showed that the annual electrical energy consumption of a supermarket can range from 100,000 to 1,500,000 kWh or even higher (2005). Supermarkets produce a considerable amount of global warming potential emissions, such as hydrofluorocarbon emissions from leaking of vapor compression cycling and CO_2 emissions from electricity originated from power stations (Cheung and Braun 2016). Thus, reducing building energy consumption for supermarkets is extremely significant.

Three approaches are available to reduce supermarket energy consumption: building improvements, HVAC system improvements, and refrigeration system display case improvements. From a building perspective, one common method to reduce energy consumption is to improve the envelope performance (e.g., better insulation) (Qian et al. 2019). HVAC systems are mainly used for indoor thermal comfort purposes for shopping customers. For HVAC systems, efficient technologies are usually preferred, such as advanced supervisory controls (e.g., model predictive controls) (Drgoňa et al. 2020). Refrigeration systems are cooling equipment used to maintain the desired food temperature for perishable goods in display cases, such as meat and dairy. For refrigerant systems, a few options to reduce energy consumption exist, including a distributed system (Sharma, Fricke, and Bansal 2014) and alternative refrigerants (Halimic et al. 2003). This study focused on transcritical CO_2 refrigeration systems.

Traditional refrigeration systems for supermarkets are either direct expansion systems or chiller systems. Many advancements have been made in reducing the energy consumption for refrigeration systems. A few major subfields include advanced operations, cooling cycle improvements, and environmentally friendly refrigerants.

Advanced operations mainly include innovative controls, optimal operation strategies, and system selections. In a previous study (Hovgaard et al. 2012), an innovative control strategy was proposed for reducing the operation cost of a supermarket refrigeration system in a virtual environment in which up to 70% power demands were achieved. Another study investigated the operation strategies to reduce the compressor cycles for distributed display cases (Ricker 2010), and the energy savings were substantial. The authors concluded that system efficiency could improve by as much as 9% by using an alternative system architecture for subcooling systems (Koeln and Alleyne 2014).

Cooling cycle improvements focus on individual components as a way to improve the overall system efficiency. In a study by (Yang and Zhang 2011)a subcooler was introduced to the two-stage system, and energy savings were found to be 27% for the R404A system and 20% for the R134a system compared with single-stage (baseline) systems (Yang and Zhang 2011). Another study found that using more subcoolers could lead to more energy savings for supermarket refrigeration systems (Koeln and Alleyne 2014). Sarkar (2012) also found that using ejectors could lead to much lower energy savings if they replace the traditional expansion valves (Sarkar 2012). Another experimental study found that the coefficient of performance increase could be 6.2% to 14.5% higher for R134a refrigerant systems (Ersoy and Sag 2014) if including ejectors in the system.

Environmentally friendly refrigerants that are also safe, stable, and energy-efficient have been studied extensively for fundamental efforts in advancing refrigeration systems. One studyreviewed numerous potential refrigerants (Calm 2008) and concluded that using a refrigerant that meets all the requirements is almost impossible (Venkatarathnam and Murthy 2012). Hydrocarbons as improved refrigerants were another intermediate solution for refrigerants. Hwang, Jin, and Radermacher (2007, 290) found that the life cycle climate performance of R410A is 4.2% lower than that of R290 refrigerants, and for R404A, the performance is 1.8% higher than that of R290 refrigerants. Another recent study (Mota-Babiloni et al. 2015) found that CO_2 refrigerant is the only refrigerant that meets the requirements described by Venkatarathnam and Murthy (2012), and it has been used in transportation refrigeration systems (Sun et al. 2014; Sun and Liu 2019; Sun et al. 2018; Sun 2019).

In recent years, more transcritical CO_2 refrigeration systems have been adopted in supermarkets (Sun, Kuruganti, et al. 2021; W. Li, Xuan, and Sun 2012). These systems are characterized by multiple benefits compared with traditional direct expansion refrigeration systems: (1) higher volumetric refrigerating capacity than other refrigerants such as chlorofluorocarbon, hydrochlorofluorocarbon, hydrofluorocarbon, and hydrocarbon refrigerants (Kim, Pettersen, and Bullard 2004); (2) no ozone depletion potential; (3) no global warming potential; and (4) nontoxic, nonflammable, and inexpensive components and emissions. (5) other aspects; One study (Ge and Tassou 2011) concluded that the lower ratio of media pressure and high-temperature compressor efficiency could lead to an increased coefficient of performance for a booster CO_2 transcritical system. Another study (Hafner, Försterling, and Banasiak 2014) found that the CO_2 refrigeration system could achieve 30% efficiency in different climate zones if ejectors and heat recovery components are added into the system. In another study, the authors compared cascade CO_2 refrigeration systems (da Silva, Bandarra Filho, and Antunes 2012) with traditional cascade refrigeration systems (R404a and R22); they concluded that CO_2 refrigeration systems have multiple merits, such as compactness, lower electricity consumption, and lower environmental impacts. Overall, CO_2 refrigeration is a low–carbon emission cooling system, superior to all other refrigerant systems, based on above 5 aspects.

However, CO_2 refrigerant systems are subject to fault operations, similar to traditional refrigeration systems (e.g., direct expansion systems). A few fault model studies exist for traditional refrigeration systems, such as fault detection and diagnostics (FDD) for rooftop units (Cheung and Braun 2015), fault impacts on chiller systems(Cheung and Braun 2016)and liquid line receiver faults of refrigerant systems (Behfar and Yuill 2020). Nevertheless, very few fault modeling studies exist for transcritical CO_2 refrigeration systems. Faults are common in buildings, and one study showed that fault conditions might lead to more than 100% energy consumption (Y. Li and O'Neill 2018). Multiple categories of faults can also occur, such as sensor faults, equipment faults, and control faults. Therefore, detecting faults is extremely important for keeping the refrigeration system operating optimally.

The three approaches to fault modeling (Y. Li and O'Neill 2018) include black-box, gray-box, and white-box. The black-box approach normally uses machine learning (data-driven) algorithms (Zhang et al. 2021), but it lacks physical details in the modeling. The white-box approach is time-consuming and labor-intensive, although it has the best fidelity (P. Li, Qiao, et al. 2014; P. Li, Li, et al. 2014). The gray-box approach combines the strengths of the black-box and white-box methods, preserving major modeling fidelity with less effort (Y. Li et al. 2021). This study applied the gray-box approach for fault modeling development for CO_2 transcritical systems. Multiple sets of experiments were conducted for the fault scenarios and baseline (fault-free) scenarios. The experiments and data sets were presented in recent publications (Fricke and Sharma 2016; Sun, Im, et al. 2021b). This study proposed multiple fault models for supermarket transcritical CO_2 refrigeration systems based on experimental data sets. These fault models were calibrated and demonstrated in a simulation environment for FDD purposes. However, no study has systematically investigated the fault modeling development and FDD applications for CO_2 refrigeration systems.

The remaining sections of this report are organized as follows. In Section 2, the overall steps used to create the fault models are discussed. Section 3 introduces the five fault models for supermarket refrigeration systems; the fault models and the baseline models are presented. In Section 4, four sets of analysis are discussed—validation of the baseline model using measurement data, presentation of the fault measurement study, calibration of fault models using measurement data, and FDD using fault models. Section 5 presents this study's conclusions.

2. METHODOLOGY

The system diagram of the transcritical CO_2 refrigeration system is shown in Figure 1. This is a two-stage system with low- and medium-temperature cooling. The specifications of the components (e.g., compressors, display case, gas cooler condenser) are shown in a previous report (Fricke and Sharma 2016). The experiments were conducted within 24 h. The measurement points are summarized by Fricke and Sharma (2016).

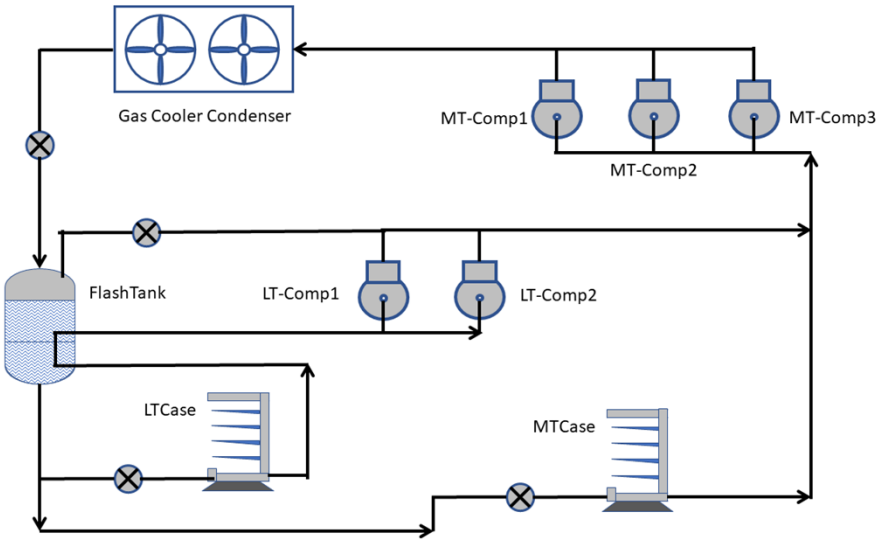

Figure 1. Transcritical CO_2 refrigeration system diagram (experiments).

For this methodology, the authors first studied the baseline (fault-free) measurement data, from which a baseline model was calibrated. Then, the baseline and fault measurement data sets were investigated, from which the fault models were developed. For the next step, FDD logics (which are used for FDD identifications) were developed. Last, the fault models were deployed into the Python EMS environment for FDD purposes. Figure 2 shows the overall framework for this study.

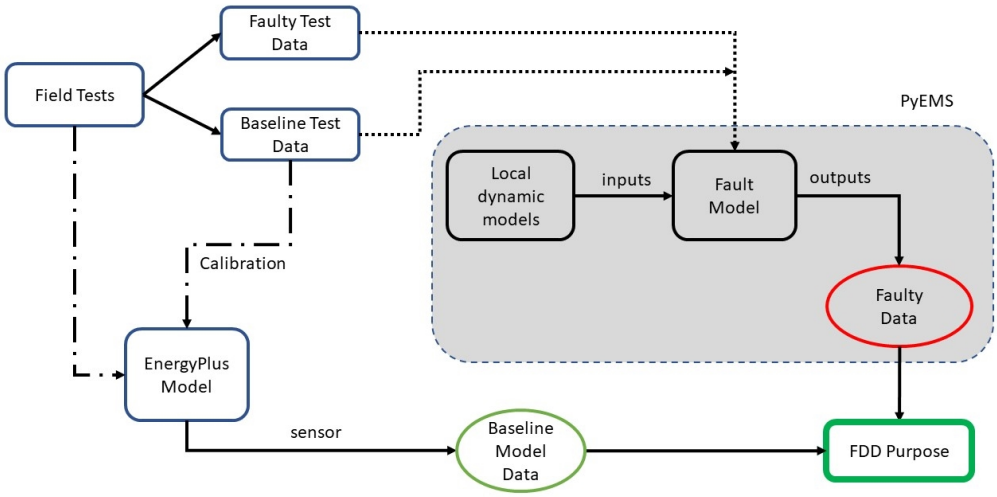

Figure 2. Fault model development framework.

3. FAULT MODELS

3.1 BASELINE MODEL

The baseline model is the model without faults. It comprises two types of compressors: low-temperature compressors and medium-temperature compressors. The metrics for the compressors are cooling capacity and power consumption.

3.1.1 Low-Temperature Compressor

The low-temperature compressor always operates at subcritical conditions. The equation is given as (AHRI 2012)

$$z = a_1 + a_2 T_o + a_3 T_c + a_4 T_o^2 + a_5 T_o T_c + a_6 T_c^2 + a_7 T_o^3 + a_8 T_c T_o^2 + a_9 T_o T_c^2 + a_{10} T_c^3 , \quad (1)$$

where

T_o is the saturated suction temperature (°C), T_c is the saturated discharge temperature (°C), z is the cooling capacity (W) or power consumption (KW), and $a_1 \sim a_{10}$ are the coefficients of the performance curve.

3.1.2 Medium-Temperature Compressor

The medium-temperature compressor operates at both subcritical and supercritical conditions. When the outdoor air temperature is lower than 88°F, the compressor will go subcritical, and when the outdoor air temperature higher than or equal to 88°F, it will go supercritical.

The supercritical equation is given as (AHRI 2012)

$$z = a_1 + a_2 T_o + a_3 P_{gc} + a_4 T_o^2 + a_5 T_o P_{gc} + a_6 P_{gc}^2 + a_7 T_o^3 + a_8 P_{gc} T_o^2 + a_9 T_o P_{gc}^2 + a_{10} P_{gc}^3 . \quad (2)$$

The subcritical equation is given as (AHRI 2012)

$$z = a_1 + a_2 T_o + a_3 T_c + a_4 T_o^2 + a_5 T_o T_c + a_6 T_c^2 + a_7 T_o^3 + a_8 T_c T_o^2 + a_9 T_o T_c^2 + a_{10} T_c^3 , \quad (3)$$

where

T_o is the saturated suction temperature (°C), T_c is the saturated discharge temperature (°C), Z is the cooling (W) or power consumption (KW), P_{gc} is the gas cooler pressure (bar), and $a_1 \sim a_{10}$ are the coefficients of the performance curve.

The baseline models provide crucial insights for the dominant parameters determining cooling capacity and power consumption for CO_2 refrigeration systems. The fault models were developed by mimicking the idea of baseline models.

3.2 FAULT MODELS

Five faults were selected for modeling because they are among the most common faults for supermarket refrigeration cases: (1) ice accumulation on the evaporator coil, (2) evaporator fan partial failure, (3) expansion valve failure, (4) display door open, and (5) condenser blockage.

3.2.1 Fault Symptoms

The following paragraphs discuss the effects of the different fault symptoms. The five faults will degrade the performance of refrigeration systems from both the air side and the refrigerant side.

Ice accumulation on the evaporator coil

On the air side, the ice will reduce the heat transfer effect of coil and thus the overall heat transfer coefficient will decrease. This fault will drive the compressor to run faster to maintain the desired set points of supply air temperature (SAT) or the set points of food temperature. This type of situation will lead to increased power demand for the compressors.

On the refrigerant side, the refrigerant temperature right after the evaporator coil may be lower than under normal conditions because of decreased heat gains from the air side. Thus, the refrigerant might not be fully evaporated or saturated with a gaseous state. Under severe fault conditions, the mixture of liquid and gases might enter the compressor and cause damage.

Evaporator fan partial failure

On the air side, the supply airflow rate will decrease; therefore, the heat transfer quantity will be decreased. On the refrigerant side, the same issue will occur with the ice accumulation on the evaporator coil model. Similarly, this fault might drive the compressor to run faster to maintain the desired set points. This fault can be detected easily with an airflow sensor.

Expansion valve failure

This fault will directly affect the refrigerant side. Normally, the purpose of the expansion valve is to reduce the pressure and temperature of the refrigerant after the condenser. Once the system is running under fault conditions, the refrigerant will carry higher than normal pressure and temperature. When the refrigerant goes through the evaporator coil, the heat transfer effect will be reduced. Thus, the SAT will be higher than normal.

Display door open

This fault is mainly imposed through the air side. When the display door is open, the indoor air (with a higher temperature) around the display case will enter through the evaporator coil. If the cooling coil capacity is not sufficiently high, the SAT will rise, even if the compressor is running at full speed. If the cooling coil capacity is sufficiently high, the compressor speed will increase to maintain the food temperature.

Condenser blockage

This fault acts on the system on the air side. The purpose of the condenser is to cool the refrigerant coming from the compressor upstream. It transfers the heating energy from the evaporator coil to the outdoor environment. When the system is running under faults, the refrigerant temperature will be higher than normal. Then, the refrigerant will go through the expansion valve with a higher temperature and, subsequently, the evaporator coil. Because of the higher temperature of the refrigerant, the heat transfer amount that is carried over is reduced. Therefore, the SAT and food temperature will be compromised.

3.2.2 Fault Model Equations

The following assumptions were made for the fault models:

- The fault condition cooling capacity is smaller than or equal to the baseline (fault-free) condition.
- The fault condition power consumption is higher than or equal to the baseline (fault-free) condition.
- The SAT of the display case is higher than or equal to the baseline (fault-free) condition.
- The fault intensity is the intensity (i.e., severity) of the fault introduced by humans (e.g., a customer forgetting to close the door of the display case) or naturally because of degradation (e.g., refrigerant leaking because the pipe eroded). This measurement indicates the severity (or fault magnitude) of the fault, and the input perturb parameter is introduced as the cause of the fault. A system may have more than one fault. The fault intensity details are given as follows:
  - Ice accumulation on the evaporator coil:
    This fault intensity was adjusted from 0 to 0.5, indicating the area of ice blocking the evaporator coil surface. Because of potential damages to the compressor, the intensity was not increased beyond 0.5.
  - Evaporator fan partial failure:
    Each evaporator has two fans. The intensity was 0.5, meaning only one fan is running. Because of potential damages to the compressor, the intensity was not increased to 1.
  - Expansion valve failure:
    The intensity was adjusted from 0 to 0.3, indicating blockage ratio. Higher blockage might lead to system refrigerant choke or compressor damage. 0 means no blockage. 1 means 100% blockage.
  - Display door open:
    The intensity was adjusted from 0 to 0.6, indicating the openness of the display door.
  - Condenser blockage:
    The intensity was adjusted from 0 to 0.5, meaning the surface area of the blockage. The higher the blockage, the smaller the area of heat exchanging through the condenser coil.
- The cooling impact ratio is the ratio between fault condition cooling capacity and baseline cooling capacity. This ratio could be an empirical value, which could be obtained from a measurement in a historical operation.
- The rated parameters are the ideal variables under nominal or normal conditions without faults, such as cooling capacity, SAT, and power.

The fault model formats and physical insights were based on multiple factors: (1) For supermarket display cases, the most important parameters are the power consumption and SAT because they directly affect the supermarket revenues and food quality, respectively. (2) The current fault models were proposed with power consumption and SAT as the top-priority variables. (3) The fault models are based on the differences between faulty and normal (or fault-free) conditions, which supermarket facilities already have. This determined the higher-level format of the fault models. (4) From actual operations and measurements, the power consumption and SAT are subject to the impacts of key parameters, including saturated suction temperature and saturated condensing temperature. Whenever a fault resides in the system, these two key variables will suffer. (5) The fault severity, or fault impact ratio, also needs to be understood because it reflects how severe the fault in the system is (e.g., a fraction number, namely the area of condenser coil blockage to the whole area of the condenser coil). Faults with higher severity tend to have higher impacts on energy consumption and supply airflow rates. (6) The equation formats are based on the 10-coefficient performance curve equations for compressors listed in the AHRI Standard 571 from the HVAC equipment manufacturers (AHRI 2012).

The fault models for both low and medium temperature display cases are based on inputs including the fault intensity, cooling impact ratio, faulty saturated suction temperature, faulty saturated condensing temperature, rated power consumption, and set of coefficients. For faulty saturated suction temperature

and faulty condensing temperature, a few additional measurements are required to construct the local dynamic models. The development of local dynamic models is shown in Eqs. (4) through (11). Figure 3 demonstrates the components of the proposed fault models.

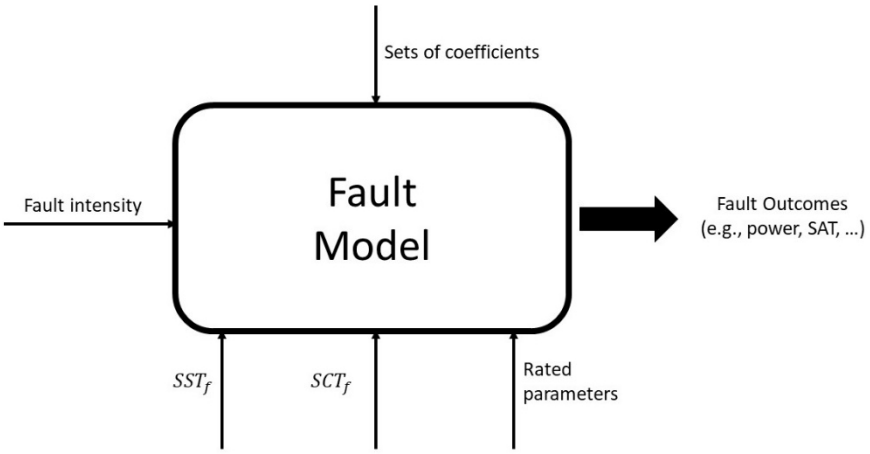

Figure 3. Fault model components.

For the cooling capacity of the display case, the lumped parameter model is shown for the baseline as

$$\dot{Q}_o = (UA)_o \times (T_{SS} - T_{ra})_o \, . \tag{4}$$

Similarly, the fault condition cooling capacity is

$$\dot{Q}_f = (UA)_f \times (T_{SS} - T_{ra})_f \, . \tag{5}$$

The ratio of the two previous cooling capacity terms is expressed as

$$\frac{\dot{Q}_f}{\dot{Q}_o} = \frac{(UA)_f \times (T_{SS} - T_{ra})_f}{(UA)_o \times (T_{SS} - T_{ra})_o} \, . \tag{6}$$

A cooling impact ratio for the cooling capacity is defined as

$$\varepsilon = \frac{\dot{Q}_f}{\dot{Q}_o} \leq 1 \, . \tag{7}$$

Another dimensionless number is the fault intensity:

$$f_i = \frac{(UA)_f}{(UA)_o} \leq 1 \, . \tag{8}$$

The formula for this intensity is given as

$$\frac{\varepsilon}{f_i} = \frac{(T_{SS} - T_{ra})_f}{(T_{SS} - T_{ra})_o} \, . \tag{9}$$

When a fault occurs on the evaporator side for the two faults chosen, the saturated suction temperature tends to increase compared with nominal conditions. Similarly, the return air temperature (RAT) tends to increase when compared with nominal conditions.

Thus, the faulty saturated suction temperature is given as

$$T_{SS_f} = \frac{\varepsilon}{f_i}\,(T_{SS} - T_{ra})_o + T_{ra_f}\,. \tag{10}$$

Following a similar approach, an equation for the faulty saturated condensing temperature can be derived as

$$T_{SC_f} = \frac{\varepsilon}{f_i}\,(T_{SC} - T_{oa})_o + T_{oa_f}\,. \tag{11}$$

The fault modes are given as follows.

Low-temperature compressor power fault model:

$$\frac{W_f}{W_n} = 1 + f_i \times \left\{c_0\,atan\left(\frac{T_{ss}}{273.15}+1\right) + c_1\left(atan\left(\frac{T_{ss}}{273.15}+1\right)\right)^2 + c_2\left(atan\left(\frac{T_{sc}}{273.15}+1\right)\right) + c_3\left(atan\left(\frac{T_{sc}}{273.15}+1\right)\right)^2 + c_4(f_i) + c_5(f_i)^2 + \right. \tag{12}$$

Medium-temperature compressor power fault model:

$$\frac{W_f}{W_n} = 1 + f_i \times \left\{c_0\,atan\left(\frac{T_{ss}}{273.15}+1\right) + c_1\left(atan\left(\frac{T_{ss}}{273.15}+1\right)\right)^2 + c_2\left(atan\left(\frac{T_{sc}}{273.15}+1\right)\right) + c_3\left(atan\left(\frac{T_{sc}}{273.15}+1\right)\right)^2 + c_4(f_i) + c_5(f_i)^2 + \right. \tag{13}$$

Low-temperature compressor SAT fault model:

$$\frac{SAT_f}{SAT_n} = 1 + f_i \times \left\{c_0\,atan\left(\frac{T_{ss}}{273.15}+1\right) + c_1\left(atan\left(\frac{T_{ss}}{273.15}+1\right)\right)^2 + c_2\left(atan\left(\frac{T_{sc}}{273.15}+1\right)\right) + c_3\left(atan\left(\frac{T_{sc}}{273.15}+1\right)\right)^2 + c_4(f_i) + c_5(f_i)^2 + \right. \tag{14}$$

Medium temperature compressor SAT fault model:

$$\frac{SAT_f}{SAT_n} = 1 + f_i \times \left\{c_0\,atan\left(\frac{T_{ss}}{273.15}+1\right) + c_1\left(atan\left(\frac{T_{ss}}{273.15}+1\right)\right)^2 + c_2\left(atan\left(\frac{T_{ss}}{273.15}+1\right)\right)^3 + c_3\left(atan\left(\frac{T_{sc}}{273.15}+1\right)\right) + c_4\left(atan\left(\frac{T_{sc}}{273.15}+\right.\right.\right. \tag{15}$$

4. RESULTS AND ANALYSIS

This section presents the results for this fault study, including the baseline field test data set, fault measurement data set, fault model calibrations, and FDD investigation with fault models. The baseline is the scenario without faults. For the fault data set, five faults were investigated: (1) ice accumulation on the evaporator coil, (2) evaporator fan partial failure, (3) expansion valve failure, (4) display door open, and (5) condenser blockage.

4.1 VALIDATION OF BASELINE MODELS AND MEASUREMENT DATA

Figure 4 demonstrates the measurement data set and modeling results for the baseline model. The red lines denote the fault measurement data set results, and the blue lines represent the fault modeling results. The top plot shows that the power consumption of the low-temperature compressor is close to the modeling results. In practical field tests, the CO_2 refrigeration systems are not operated at 100% efficiency, which leads to small biases between the measurement data set and modeling results. The bottom plot is for the medium-temperature compressor. Discrepancies also exist between the field test data sets and modeling because of the nonoptimal running conditions (e.g., outdoor air temperature). However, the overall trends agreed well between the measurement and modeling results for the medium-temperature compressor.

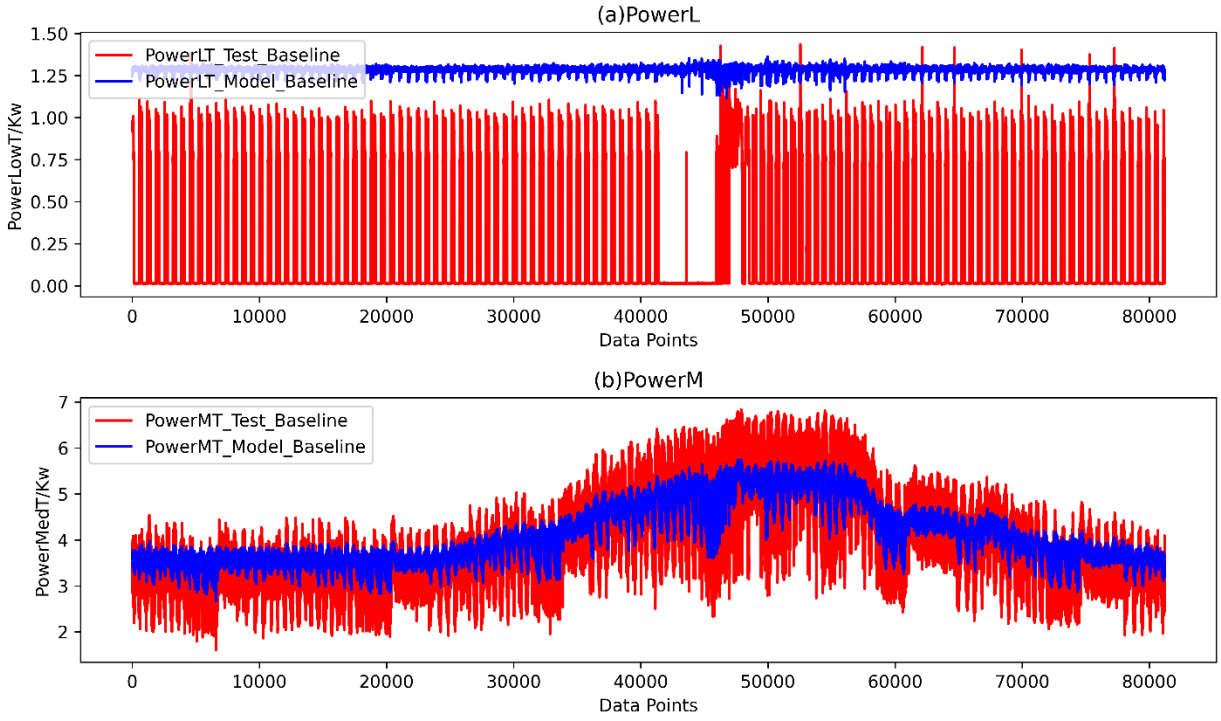

Figure 4. Comparison of the baseline measurement and model.

4.2 FAULTS MEASUREMENT DATA STUDY

This section summarizes the analysis for the fault measurement data. In figures, the red lines denote the baseline results, and the blue lines denote the fault results. For each row, the left subplot is for low-temperature compressors, and the right subplot is for medium-temperature compressors.

4.2.1 Ice Accumulation on the Evaporator Coil

Figure 5 demonstrates the measurement data sets for fault and normal conditions for ice accumulation on the evaporator coil.

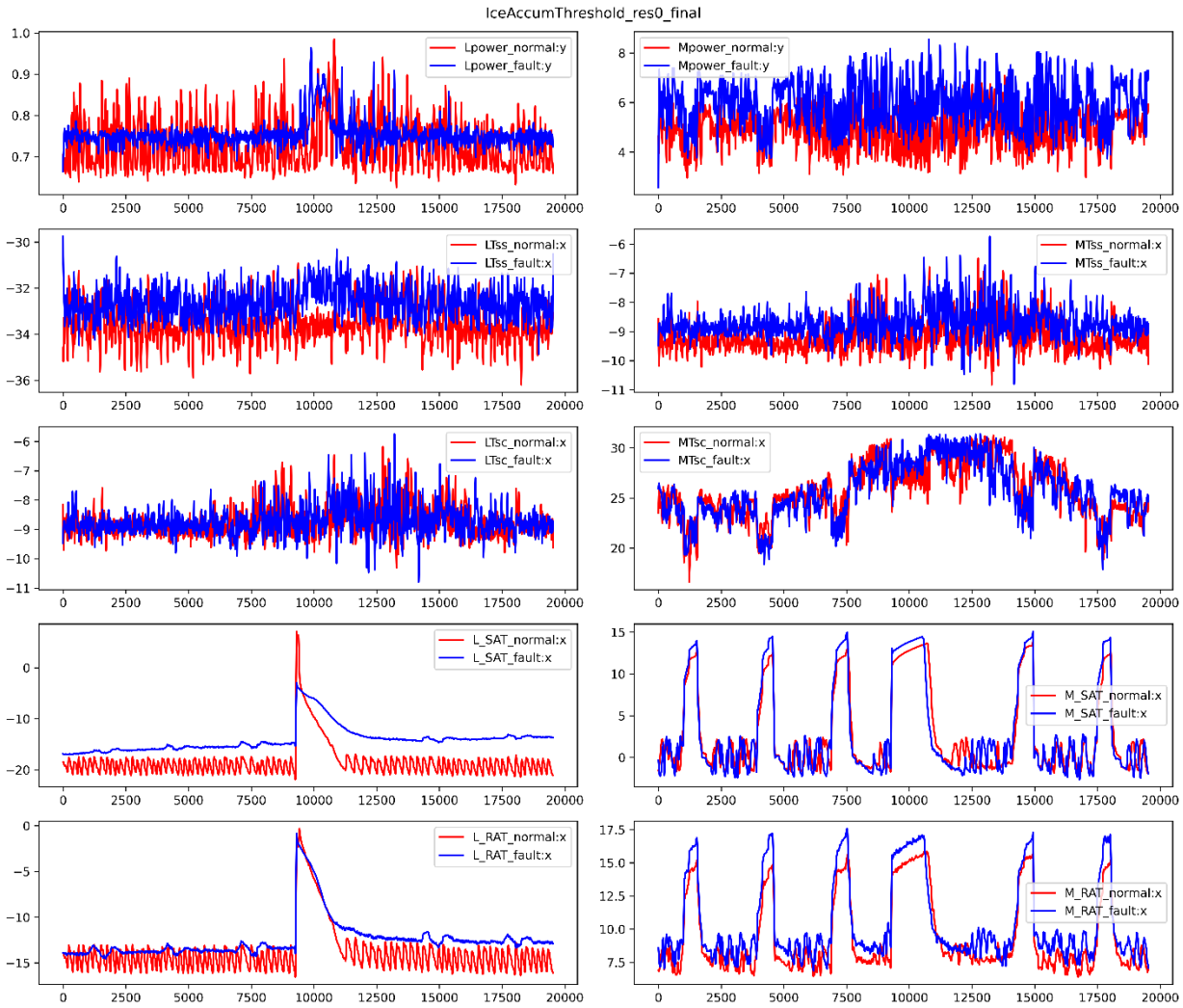

Figure 5. Ice accumulation on the evaporator coil fault measurement for fault and normal conditions.

The first row shows the power consumption for low- and medium-temperature compressors. Because of the dynamic nature of system operation, observing the differences in power consumption is difficult. However, the average power consumption for the fault condition is generally higher than for the normal condition.

The second row shows the saturated suction temperature for low- and medium-temperature compressors. Similarly to power consumption, the average saturated suction temperature for the fault condition was higher than for the normal condition.

The third row shows the saturated condensing temperature for low- and medium-temperature compressors. The differences between the fault and normal conditions are very small.

The fourth row shows the SAT for low- and medium-temperature compressors. The low-temperature compressors under the fault condition have a higher SAT than the normal condition. For medium-temperature compressors, the differences in SAT are smaller between the fault and normal conditions.

The fifth row shows the RAT for low- and medium-temperature compressors. The RAT has the same patterns as the SAT. Notably, the RAT for medium-temperature compressors has larger discrepancies between the normal and fault conditions.

4.2.2 Evaporator Fan Partial Failure

Figure 6 demonstrates the measurement data sets for fault and normal conditions for evaporator fan partial failure.

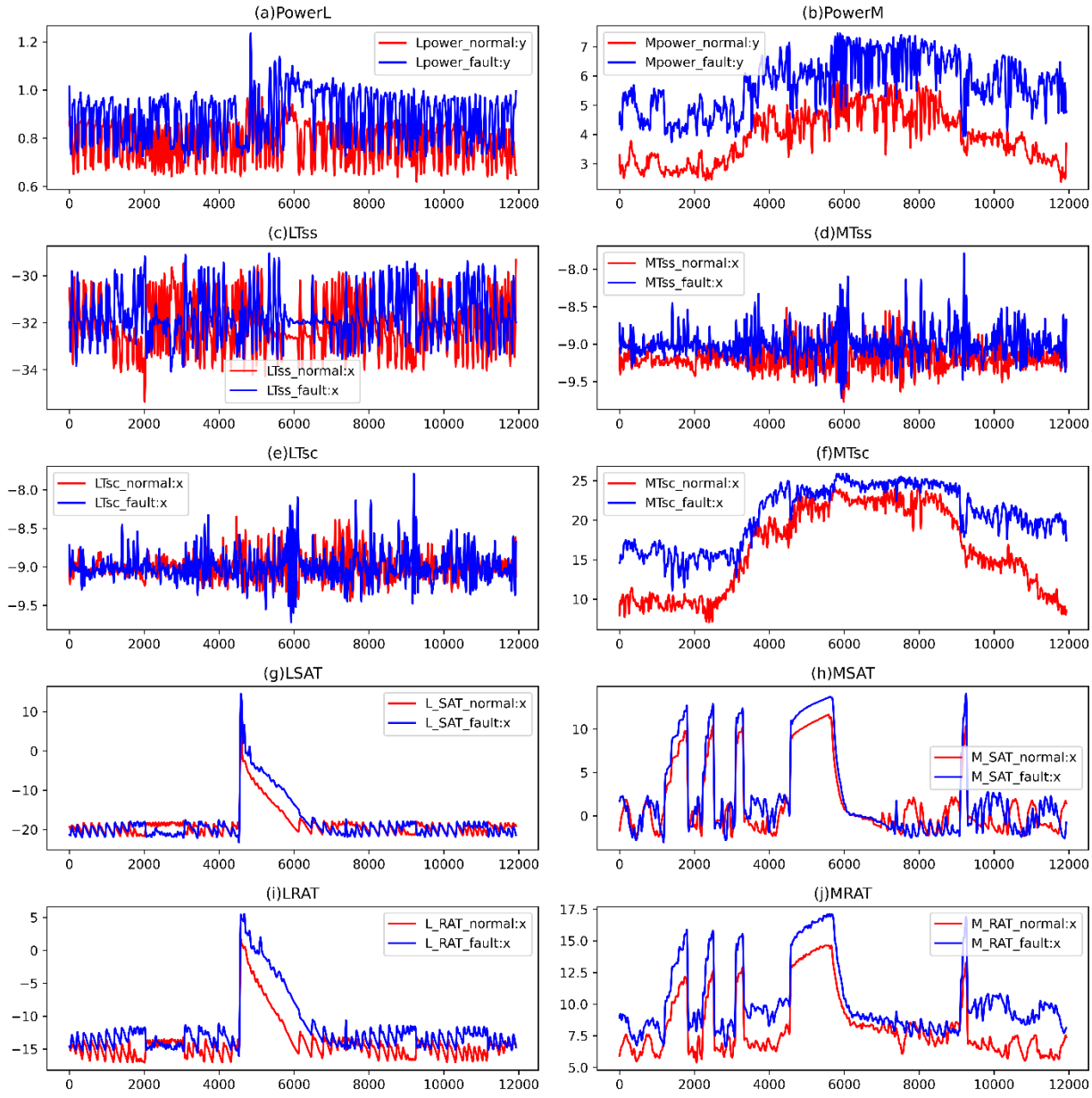

Figure 6. Evaporator fan partial failure measurement for fault and normal conditions.

The first row shows the power consumption for low- and medium-temperature compressors. Observing the differences in power consumption for low-temperature compressors is difficult. The differences in power consumption are higher for the medium-temperature compressor.

The second row shows the saturated suction temperature for low- and medium-temperature compressors. For medium-temperature compressors, the fault condition has a higher than normal condition for the saturated suction temperature. For low-temperature compressors, the differences are difficult to ascertain.

The third row shows the saturated condensing temperature for low- and medium-temperature compressors. The differences between the fault and normal conditions are very small for the low-temperature compressor. The discrepancies for medium-temperature compressors are greater.

The fourth row shows the SAT for low- and medium-temperature compressors. The differences in the SAT are difficult to recognize between the fault and normal conditions.

The fifth row shows the RAT for low- and medium-temperature compressors. The RAT has the same patterns as the SAT. Both the low- and medium-temperature compressors have larger discrepancies of RAT and SAT between normal and fault conditions.

4.2.3 Expansion Valve Failure

Figure 7 demonstrates the measurement data sets for fault and normal conditions for expansion valve failure.

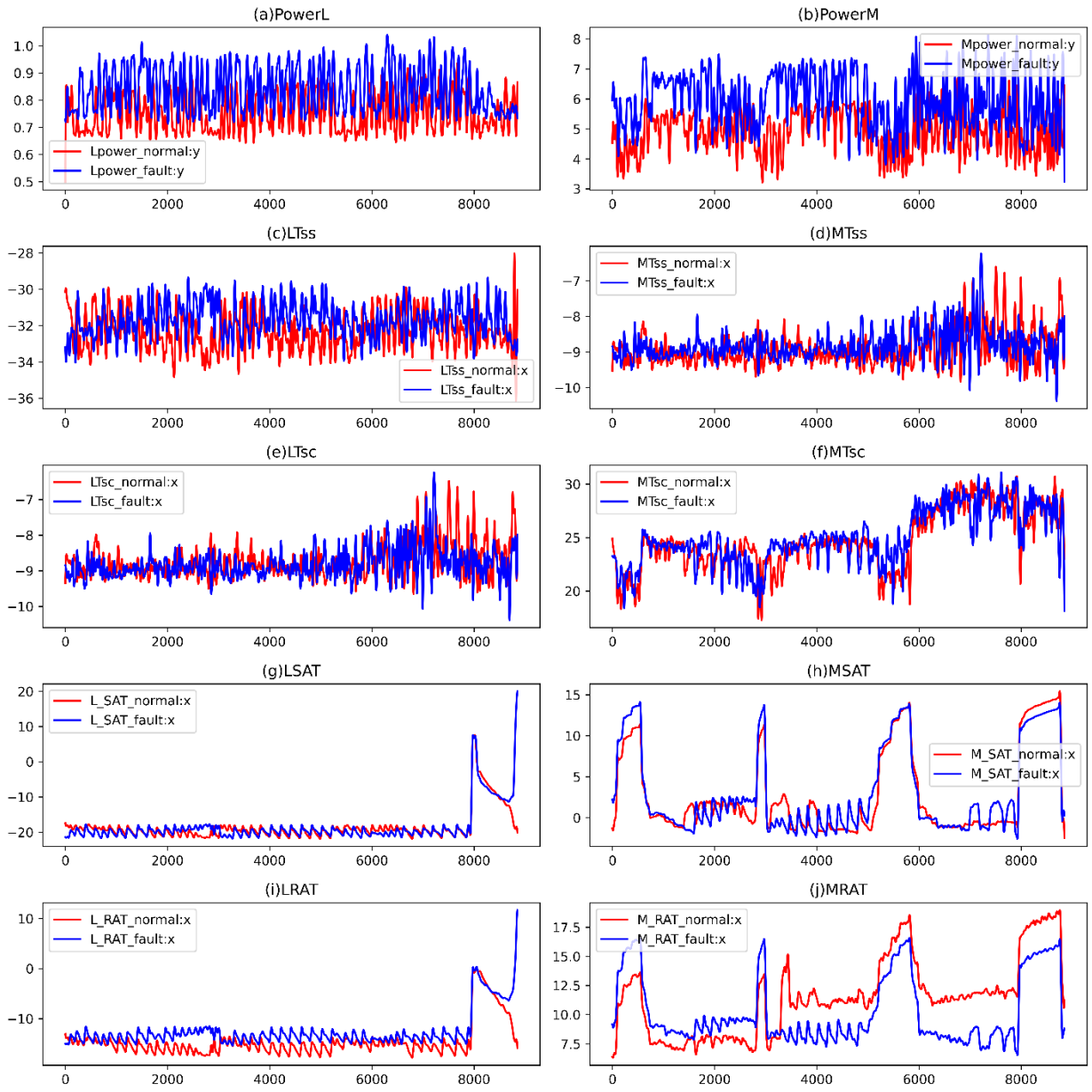

Figure 7. Expansion valve failure fault measurement for fault and normal conditions.

The first row shows the power consumption for low- and medium-temperature compressors. The differences in power consumption are evident for the low-temperature compressor.

The second row shows the saturated suction temperature for low- and medium-temperature compressors. For medium-temperature compressors, the fault condition shows little difference compared with normal conditions for the saturated suction temperature. For low-temperature compressors, the differences are clear.

The third row shows the saturated condensing temperature for low- and medium-temperature compressors. The differences between fault and normal conditions are very small for both compressors.

The fourth row shows the SAT for low- and medium-temperature compressors. The differences in the SAT are difficult to recognize between the fault and normal conditions.

The fifth row shows the RAT for low- and medium-temperature compressors. The RAT has the same patterns as the SAT. Both the low- and medium-temperature compressors have larger discrepancies between normal and fault conditions.

4.2.4 Display Door Open

Figure 8 demonstrates the measurement data sets for fault and normal conditions for display door open.

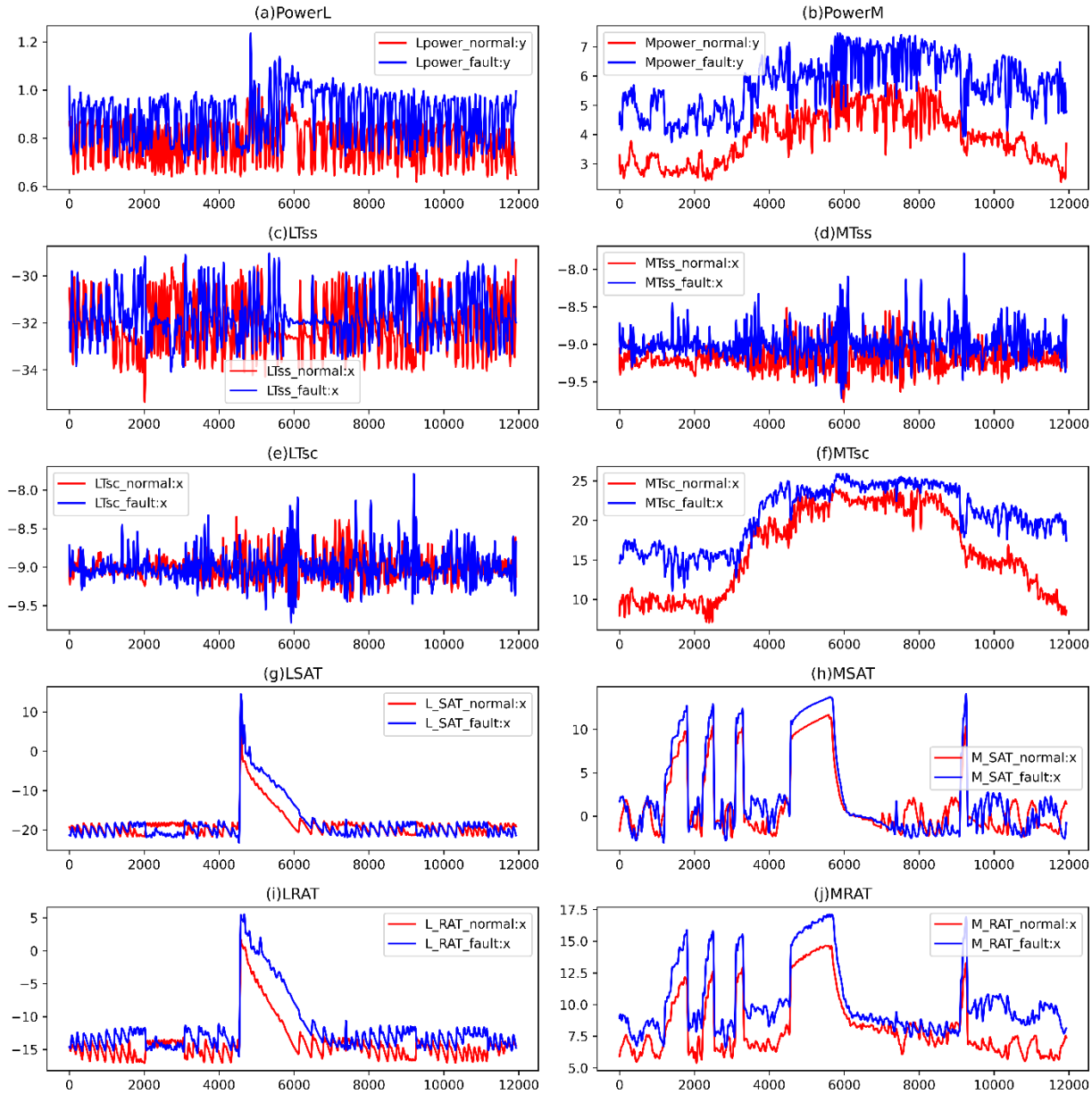

Figure 8. Display door open fault measurement for fault and normal conditions.

The first row shows the power consumption for low- and medium-temperature compressors. Observing the differences in power consumption for low-temperature compressors is difficult. The differences in power consumption for medium-temperature compressors are greater.

The second row shows the saturated suction temperature for low- and medium-temperature compressors. For medium-temperature compressors, the fault condition has a higher than normal condition for the saturated suction temperature. For low-temperature compressors, the differences are more difficult to determine.

The third row shows the saturated condensing temperature for low- and medium-temperature compressors. The differences between fault and normal conditions are very small for low-temperature compressors. The discrepancies for medium-temperature compressors are greater.

The fourth row shows the SAT for low- and medium-temperature compressors. SAT differences are difficult to recognize between fault and normal conditions.

The fifth row shows the RAT for low- and medium-temperature compressors. The RAT has the same patterns as the SAT. Both the low- and medium-temperature compressors have larger discrepancies between normal and fault conditions.

4.2.5 Condenser Blockage

Figure 9 demonstrates the measurement data sets for fault and normal conditions for condenser blockage.

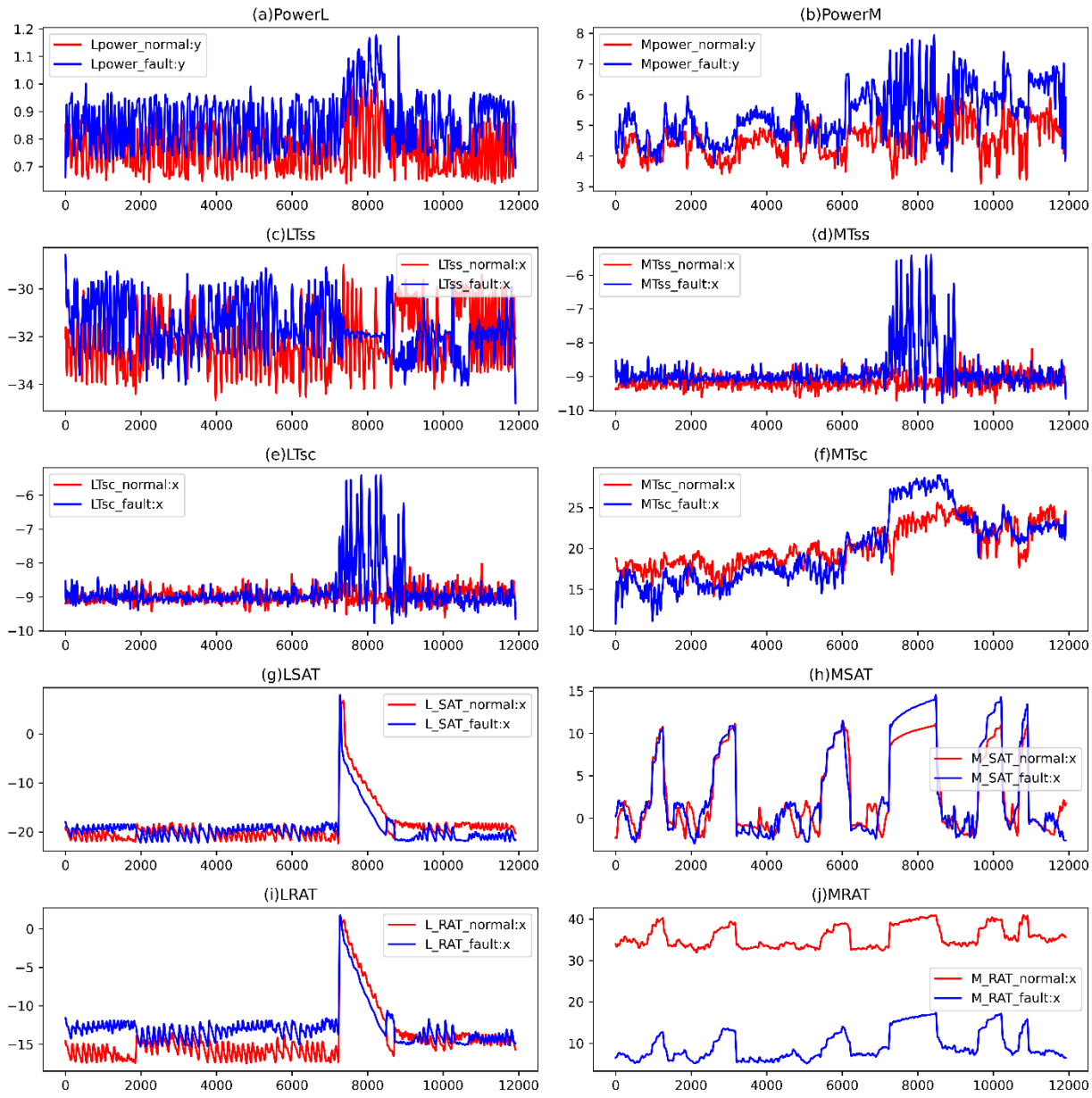

Figure 9. Condenser blockage measurement for fault and normal conditions.

The first row shows the power consumption for low- and medium-temperature compressors. Power consumption differences are obvious for both compressors.

The second row shows the saturated suction temperature for low- and medium-temperature compressors. For medium-temperature compressors, the fault condition has higher than normal condition for the saturated suction temperature. For low-temperature compressors, the differences are difficult to ascertain.

The third row shows the saturated condensing temperature for low- and medium-temperature compressors. The differences between fault and normal conditions are very small for low-temperature compressors. The discrepancies for medium-temperature compressors are greater.

The fourth row shows the SAT for low- and medium-temperature compressors. The differences in the SAT are difficult to recognize between fault and normal conditions.

The fifth row shows the RAT for low- and medium-temperature compressors. The RAT has the same patterns as the SAT. Both the low- and medium-temperature compressors have larger discrepancies between normal and fault conditions.

For brevity, other faults are not displayed here. Detailed comparisons between the baseline and each fault are provided in earlier publications (Sun, Im, et al. 2021a; 2021b). The comparisons include (1) the power consumption for low- and medium-temperature compressors, (2) the saturated suction temperature for low- and medium-temperature compressors, (3) the saturated condensing temperature for low- and medium-temperature compressors, (4) the SAT for low- and medium-temperature compressors, and (5) the RAT for low- and medium-temperature compressors.

4.3 CALIBRATION OF FAULTS MODELS USING MEASUREMENT DATA

This section demonstrates the calibrations of fault models based on measurement data sets. In figures, the red lines denote the fault measurement data set, and the blue lines represent the fault modeling data set. The upper row subplots show the power consumption for low- and medium-temperature compressors. The bottom row subplots show the SAT for low- and medium-temperature compressors. The root mean square error (RMSE) was used to quantify the discrepancies between measurement and modeling results.

4.3.1 Ice Accumulation on the Evaporator Coil

Figure 10 demonstrates the comparison of fault model results and fault measurement data set results for the ice accumulation on the evaporator coil fault. The RMSE was used to determine the modeling agreement with the measurement data set. The power consumption for the low-temperature and medium-temperature cases agree well. For the SAT, the fault model also closely follows the patterns captured from the measurement data set.

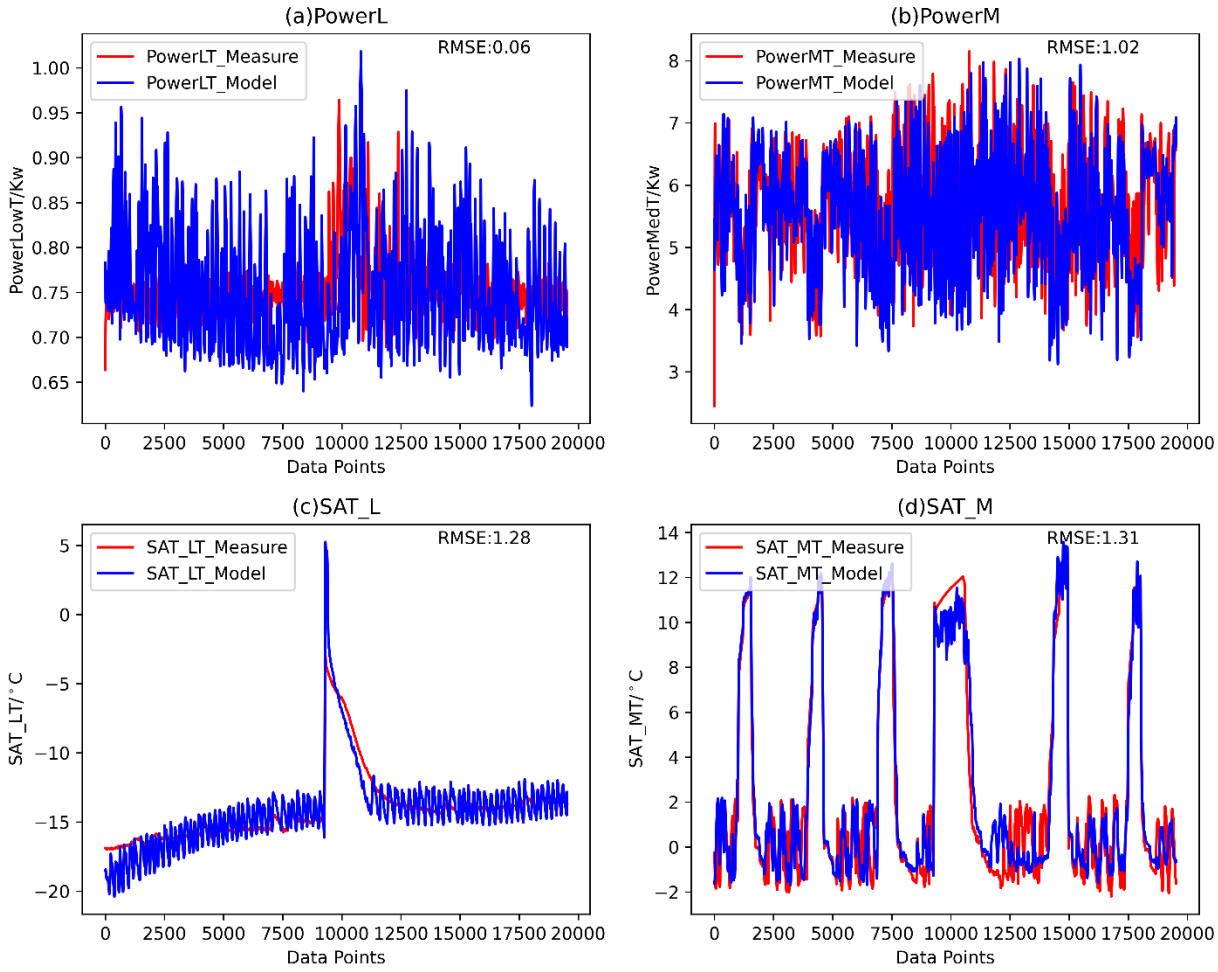

Figure 10. Calibration of ice accumulation for the evaporator fault.

4.3.2 Evaporator Fan Partial Failure

Figure 11 demonstrates the comparison of fault model results and fault measurement data set results for the evaporator fan partial failure fault. As shown in the plots, the RMSEs are both acceptable. The power consumption and SAT are in good agreement between the fault models and measurement data sets.

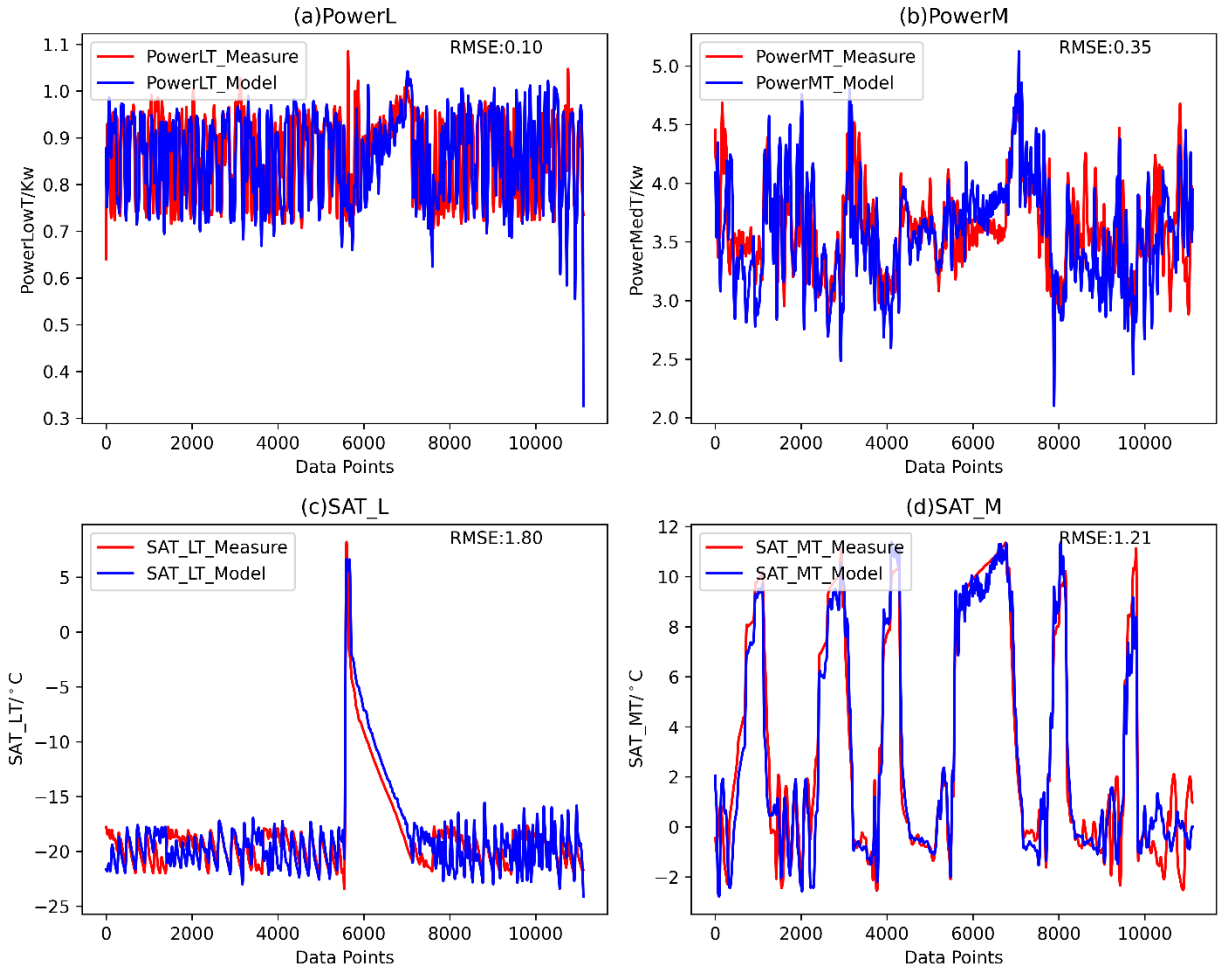

Figure 11. Calibration for the evaporator fan partial failure fault.

4.3.3 Expansion Valve Failure

Figure 12 demonstrates the comparison of fault model results and fault measurement data set results for the expansion valve failure fault. As shown in the plots, the RMSEs are both acceptable. For power consumption, the fault modeling results are close to the measurement data set. For SAT prediction in the medium-temperature display case, the fault model lacks dynamics compared with the measurement data set. However, the RMSE indicates it is acceptable for the fault models regarding the SAT.

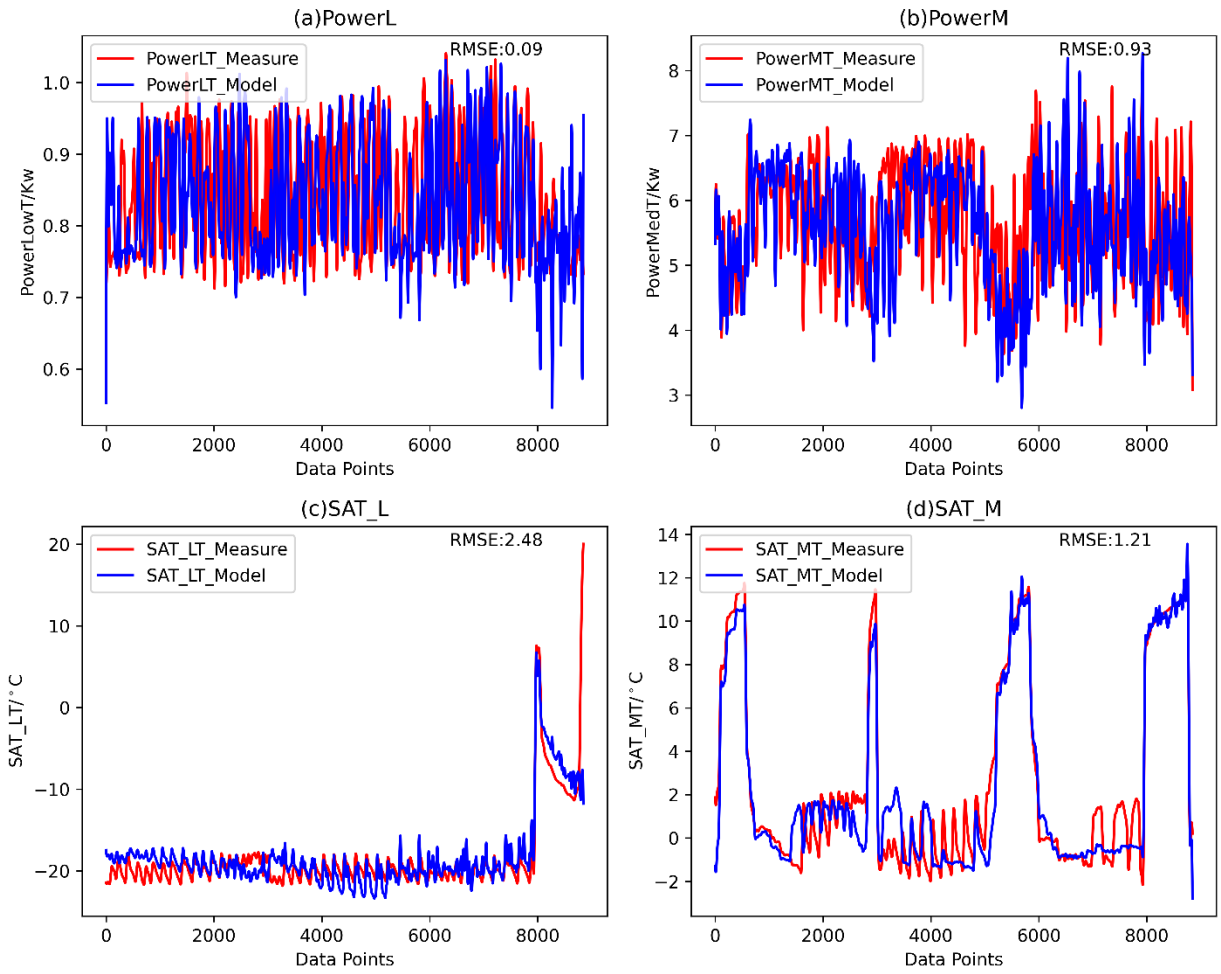

Figure 12. Calibration for the expansion valve failure fault.

4.3.4 Display Door Open

Figure 13 demonstrates the comparison of fault model results and fault measurement data set results for the display door open fault. As shown in the plots, the RMSEs are both acceptable. Overall, the fault model results are close to measurement data set results. In some small portions of the data set, the dynamics are not captured well, perhaps because of measurement noise or system dynamics.

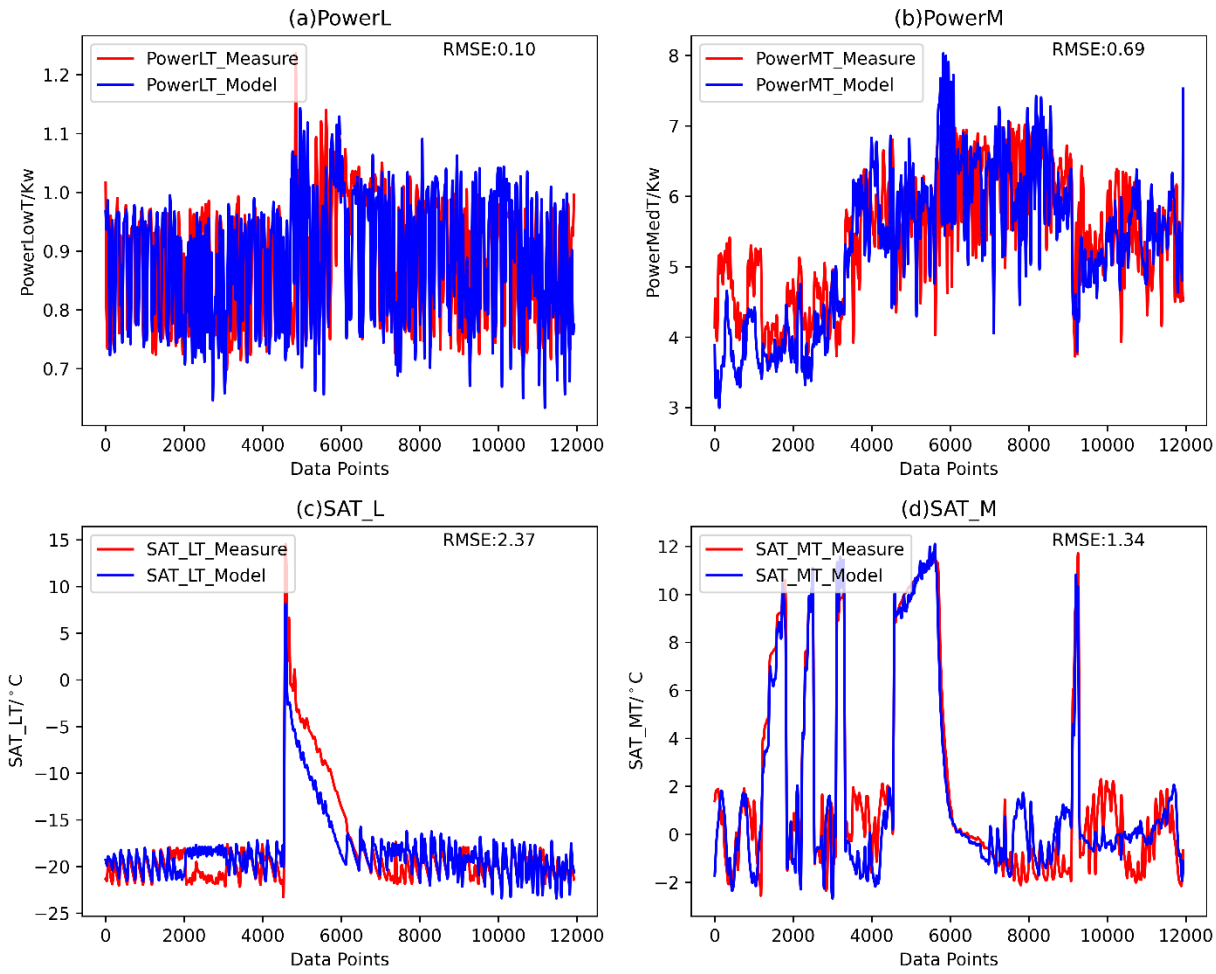

Figure 13. Calibration for the display door open fault.

4.3.5 Condenser Blockage

Figure 14 demonstrates the comparison of fault model results and fault measurement data set results for the condenser blockage fault. As shown in the plots, the RMSEs are both acceptable. The power consumption and SAT results agree well between the fault models and measurement data set.

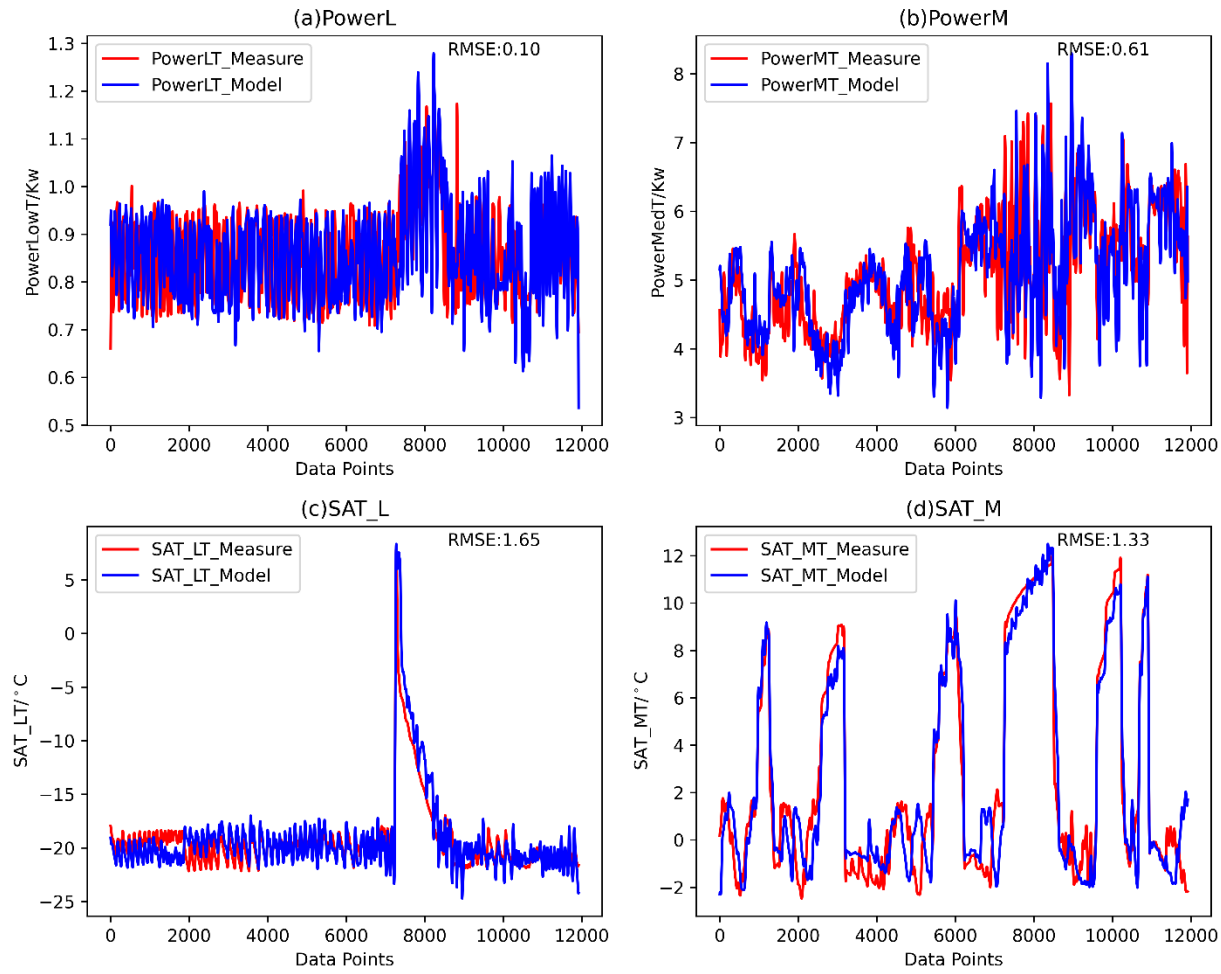

Figure 14. Calibration for the condenser blockage fault.

4.4 IMPLEMENTATION OF FAULT MODELS IN PYTHON EMS

This section summarizes the fault modeling implementation through Python EMS. In figures, the red lines denote the baseline results, and the blue lines denote the fault results. Three days of simulation results were retrieved and implemented. The top plots are for the power consumption of low- and medium-temperature compressors. The bottom plots are for the SAT of low- and medium-temperature compressors.

4.4.1 Ice Accumulation on the Evaporator Coil

Figure 15 demonstrates the fault modeling results in the EnergyPlus environment for the ice accumulation on the evaporator coil fault. A larger difference for power and SAT exists between the baseline and fault conditions. The fault results show higher power consumption than the baseline. The results are similar for SAT. Furthermore, with a decreasing SAT, the power consumption increases. From a modeling perspective, this indicates that the refrigeration is working harder to achieve the set points.

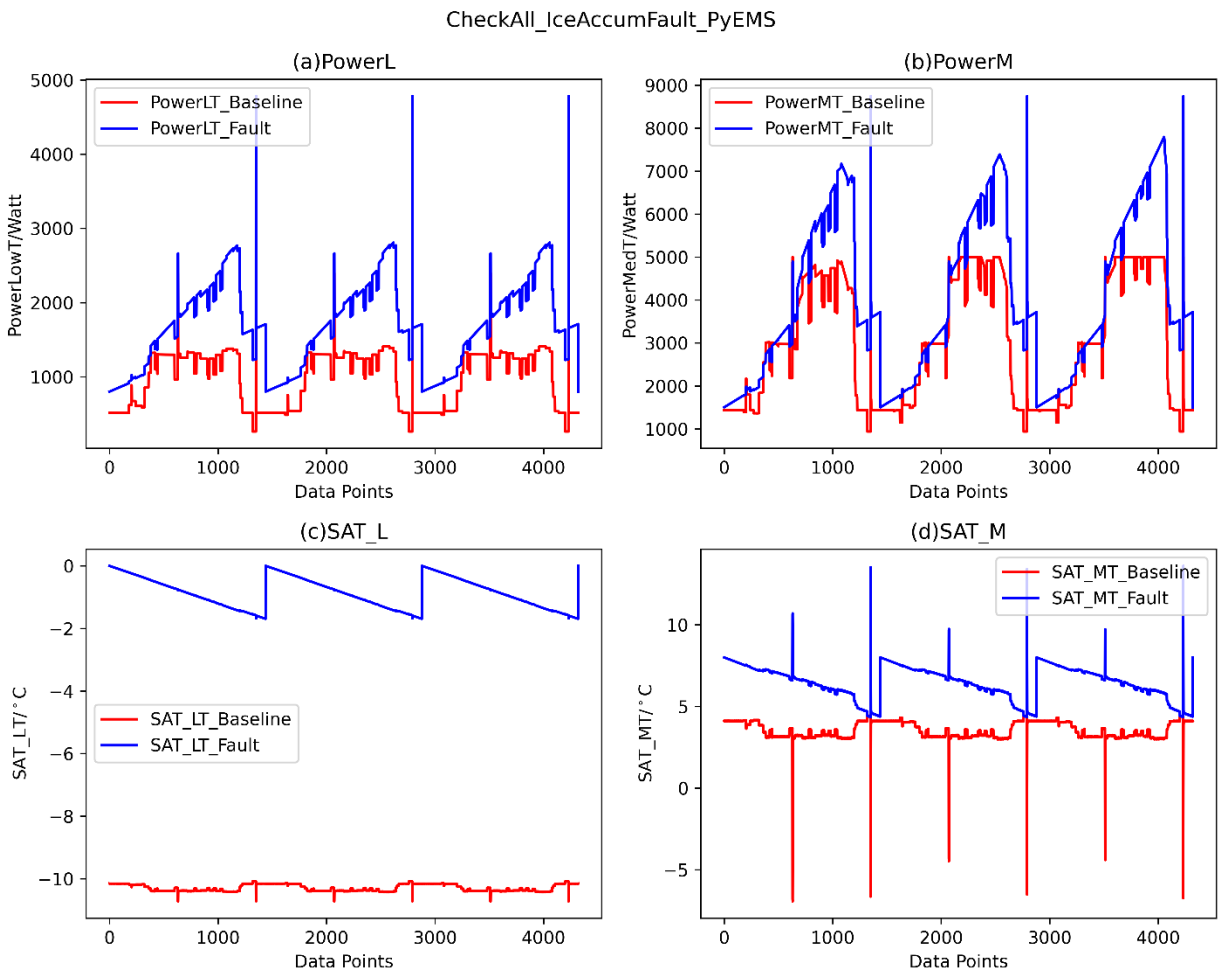

Figure 15. EnergyPlus implementation for the ice accumulation on the evaporator coil fault.

4.4.2 Evaporator Fan Partial Failure

Figure 16 demonstrates the fault modeling results in the EnergyPlus environment for the evaporator fan partial failure fault. A larger difference exists between the baseline and fault conditions. The fault case shows higher values for power consumption and SAT compared with the baseline.

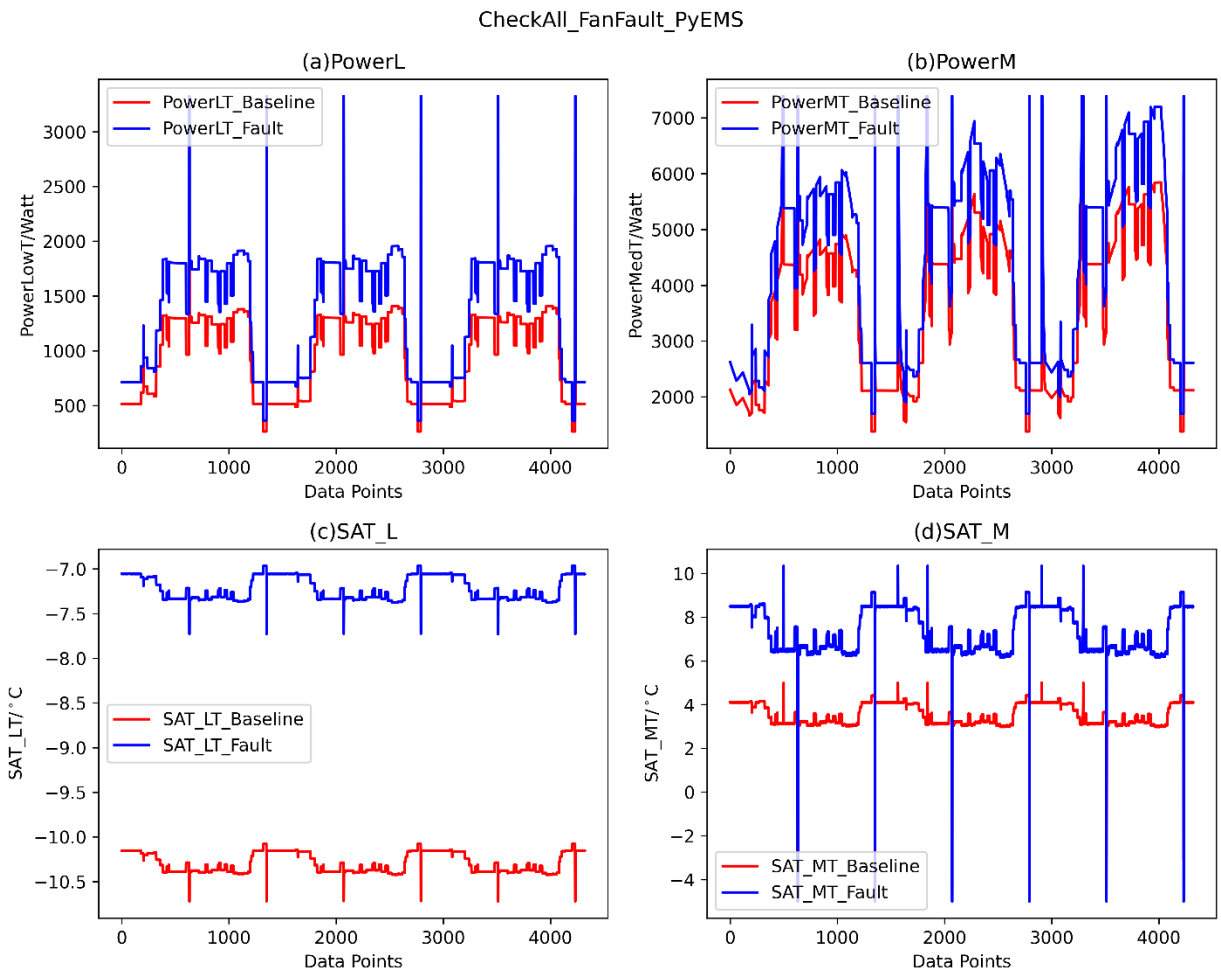

Figure 16. EnergyPlus implementation for the evaporator fan partial failure fault.

4.4.3 Expansion Valve Failure

Figure 17 demonstrates the fault modeling results in the EnergyPlus environment for the expansion valve failure fault. A larger difference exists between the baseline and fault conditions. This fault behavior is similar to the ice accumulation on the evaporator coil fault. With a decreasing SAT, the power consumption increases. The SAT in the fault condition never achieved the SAT in the baseline.

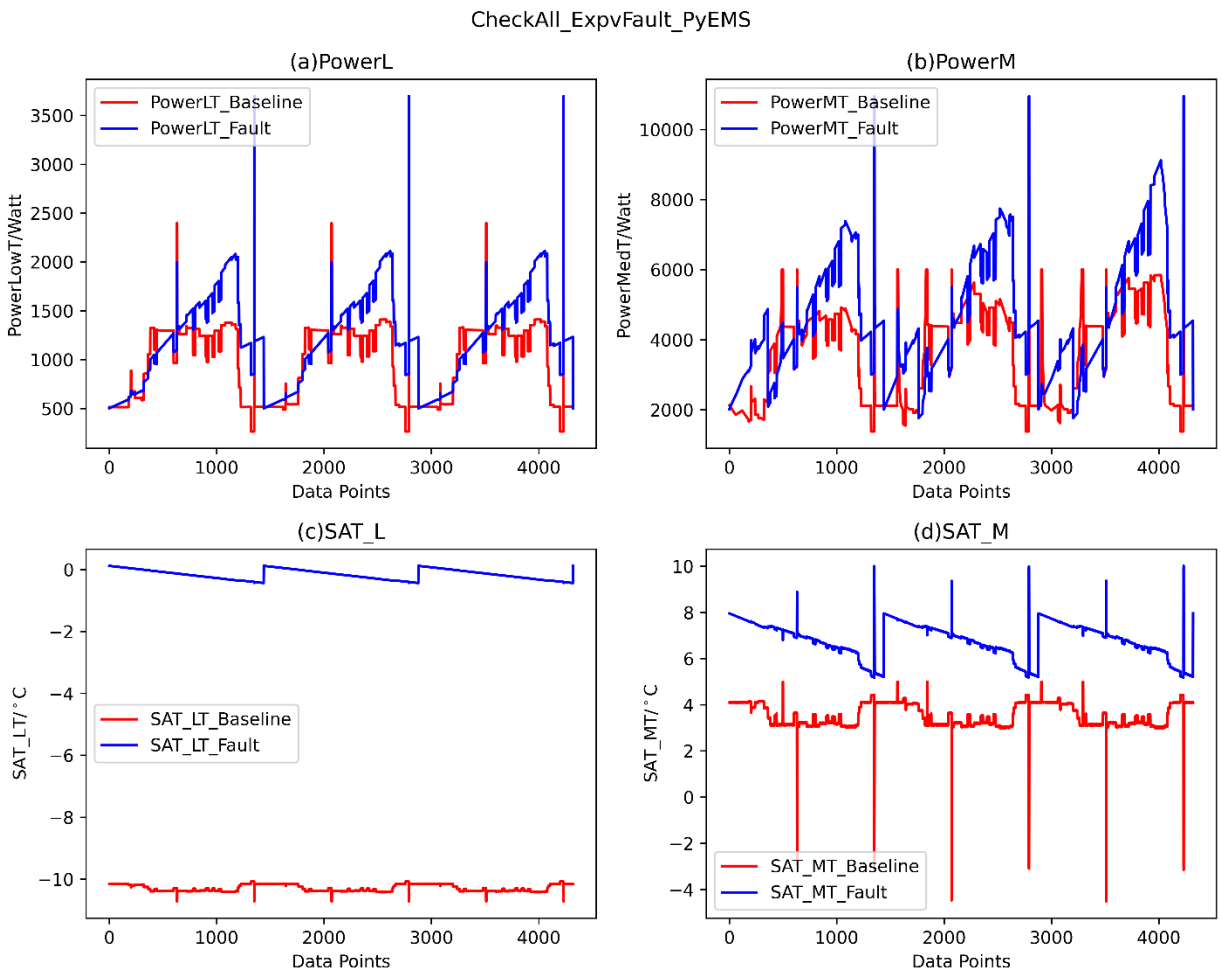

Figure 17. EnergyPlus implementation for the expansion valve failure fault.

4.4.4 Display Door Open

Figure 18 demonstrates the fault modeling results in the EnergyPlus environment for the display door open fault. A larger difference exists between the baseline and fault conditions. Similarly to the expansion valve failure fault, the power consumption and SAT of the fault models are higher than in the baseline.

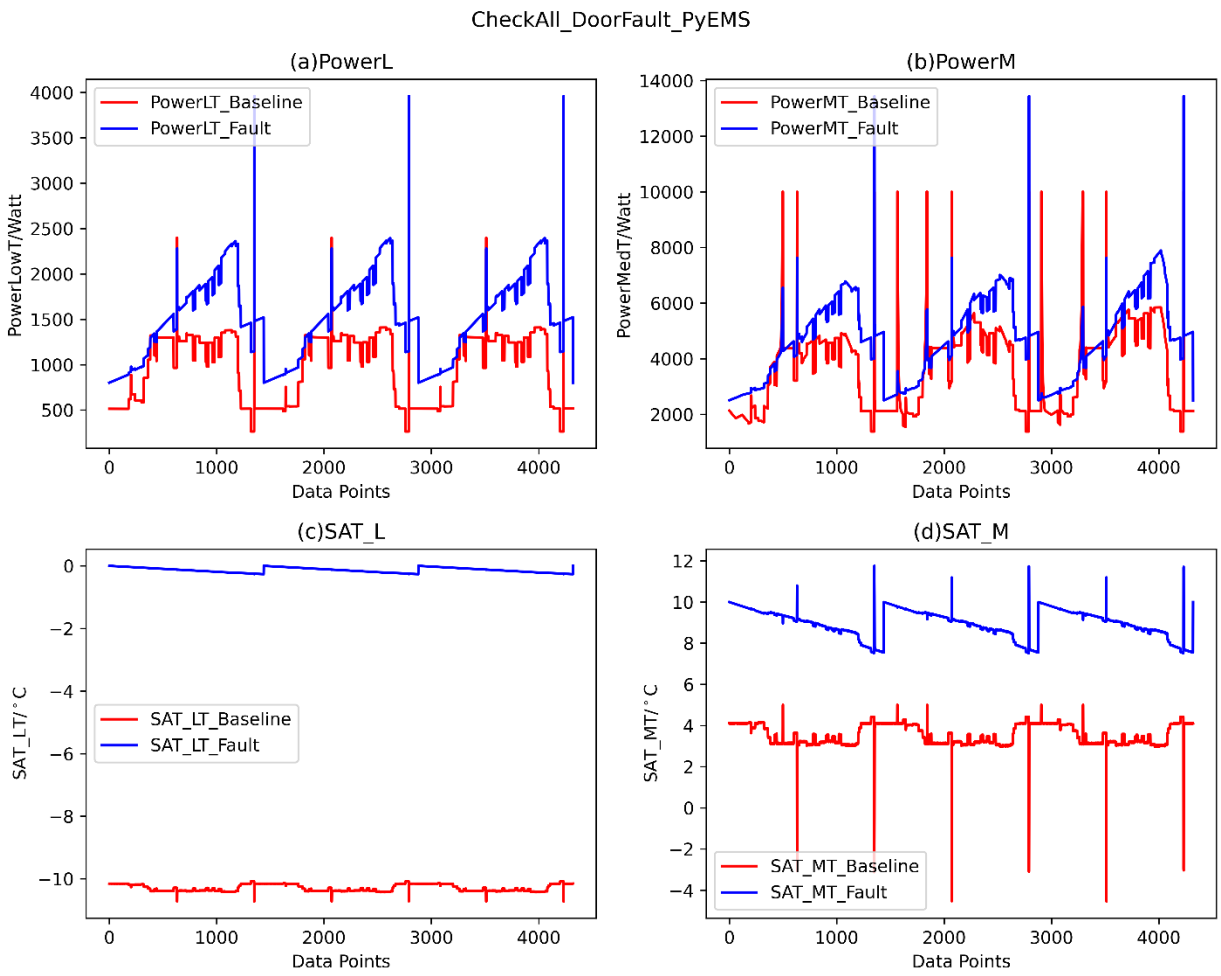

Figure 18. EnergyPlus implementation for the display door open fault.

4.4.5 Condenser Blockage

Figure 19 demonstrates the fault modeling results in the EnergyPlus environment for the condenser blockage fault. A larger difference exists between the baseline and fault conditions.

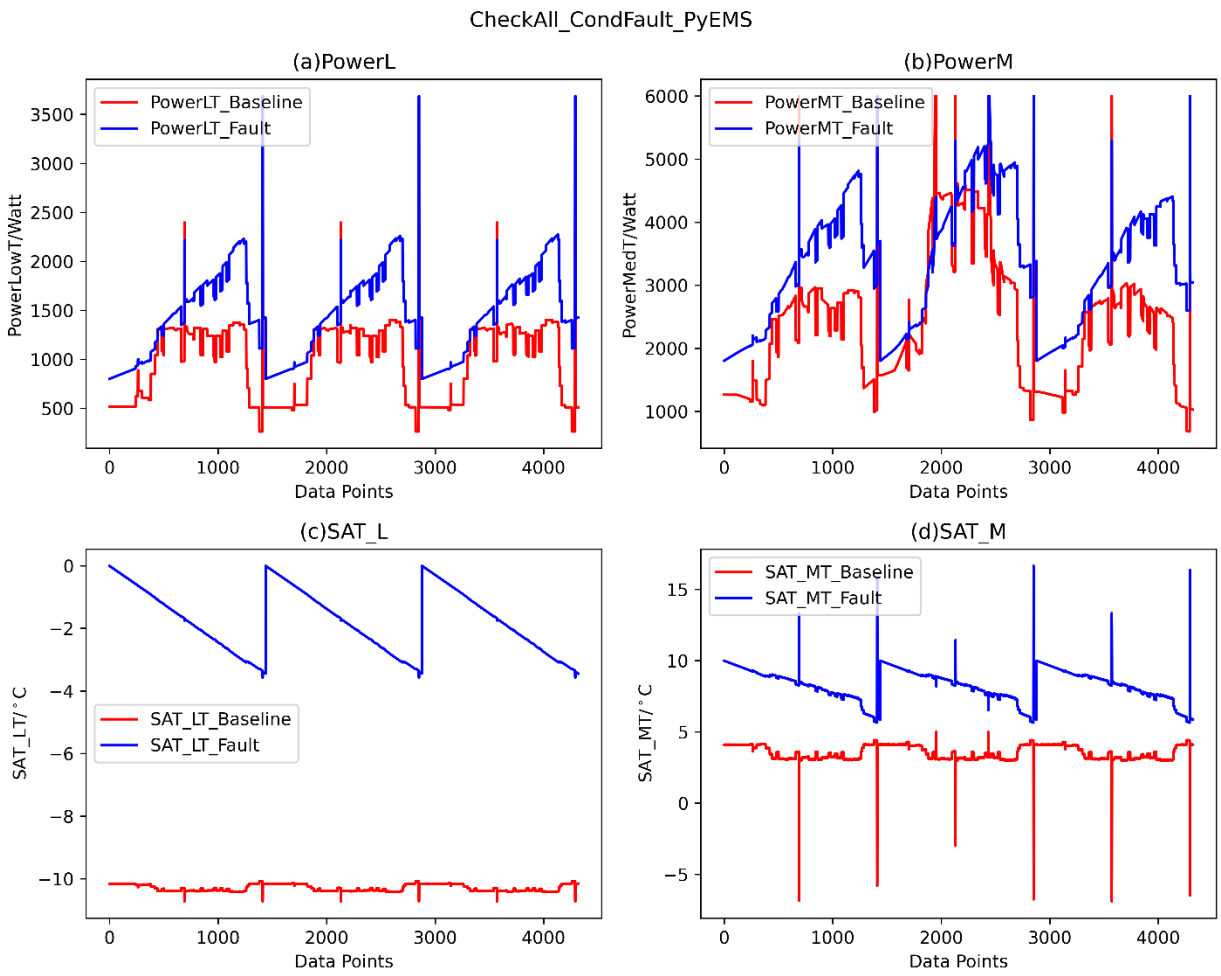

Figure 19. EnergyPlus implementation for the condenser blockage fault.

4.5 FDD USING FAULT MODELS

The purpose of fault model development is to perform FDD in the systems. An FDD algorithm was developed based on measurement data.

4.5.1 FDD Algorithm

Detecting faults for CO_2 refrigeration systems is complicated, so the authors developed an FDD flow chart based the field tests (Figure 20). The principle of FDD is shown in Figure 21. The FDD is obtained based on measurement data from both the air and refrigerant sides. Compressor faults are not included in this study. Based on the FDD flow chart, seven different indicators exist:

0: No fault
1: Evaporator fan fault
2: Display case door fault
3: Expansion valve fault
4: Condenser fault or compressor fault
5: Condenser fan fault
6: Evaporator fault

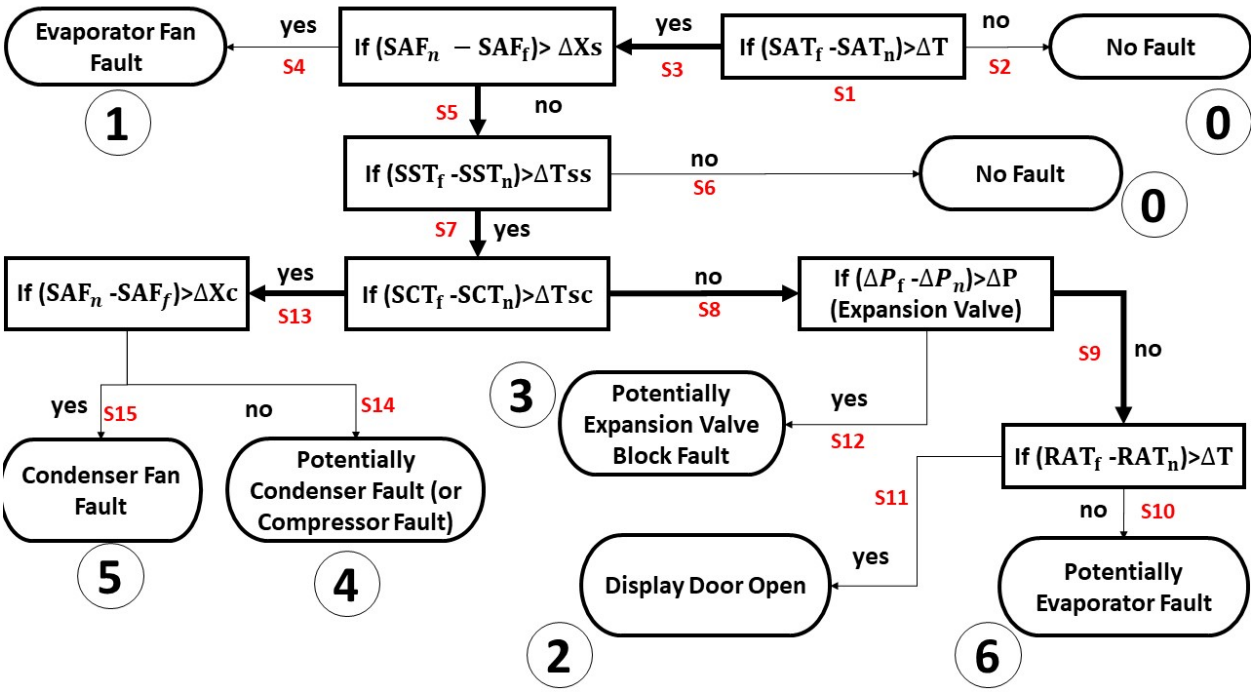

Figure 20. FDD flow chart.

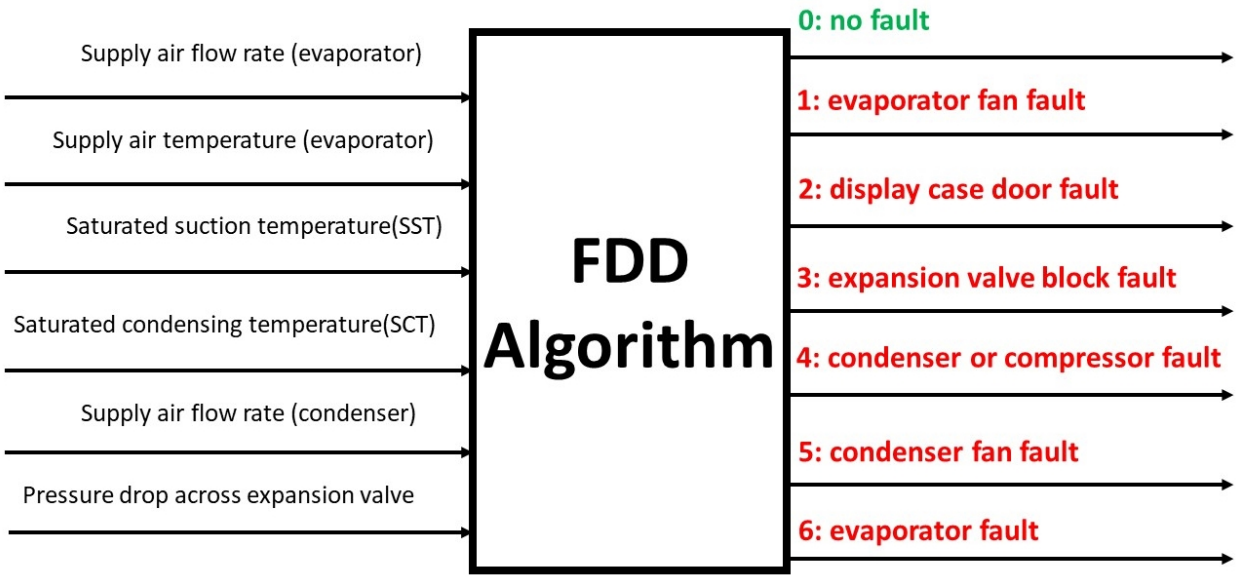

Figure 21. FDD principle.

A decision tree format was followed for fault model detection. As shown in Figure 20, the red symbols (S1–S15) are the steps to follow. The FDD starts with S1 and traverses all the way to S15 for completeness. If a fault is identified during the middle, there is no need to go through all the way to the last step (S15).

Because of time limitations, the measurement points only cover major variables. More variables need to be collected for a better FDD algorithm. The FDD algorithm is a decision tree type flow chart with different thresholds and branches. The FDD algorithm aims to automatically detect faults (currently for

the five selected faults). To develop a more comprehensive FDD algorithm, more measuring points are needed, including the temperature/pressure values before and after each major component of the refrigeration systems. This development will be included in future research.

4.5.2 FDD for Measurement Data Set

Figure 22 demonstrates the FDD results for the measurement data for the five faults investigated. The FDD value of 0 denotes the fault-free condition. The FDD value of greater than 0 indicates the fault types as proposed in the FDD algorithm, as shown in Figure 21.

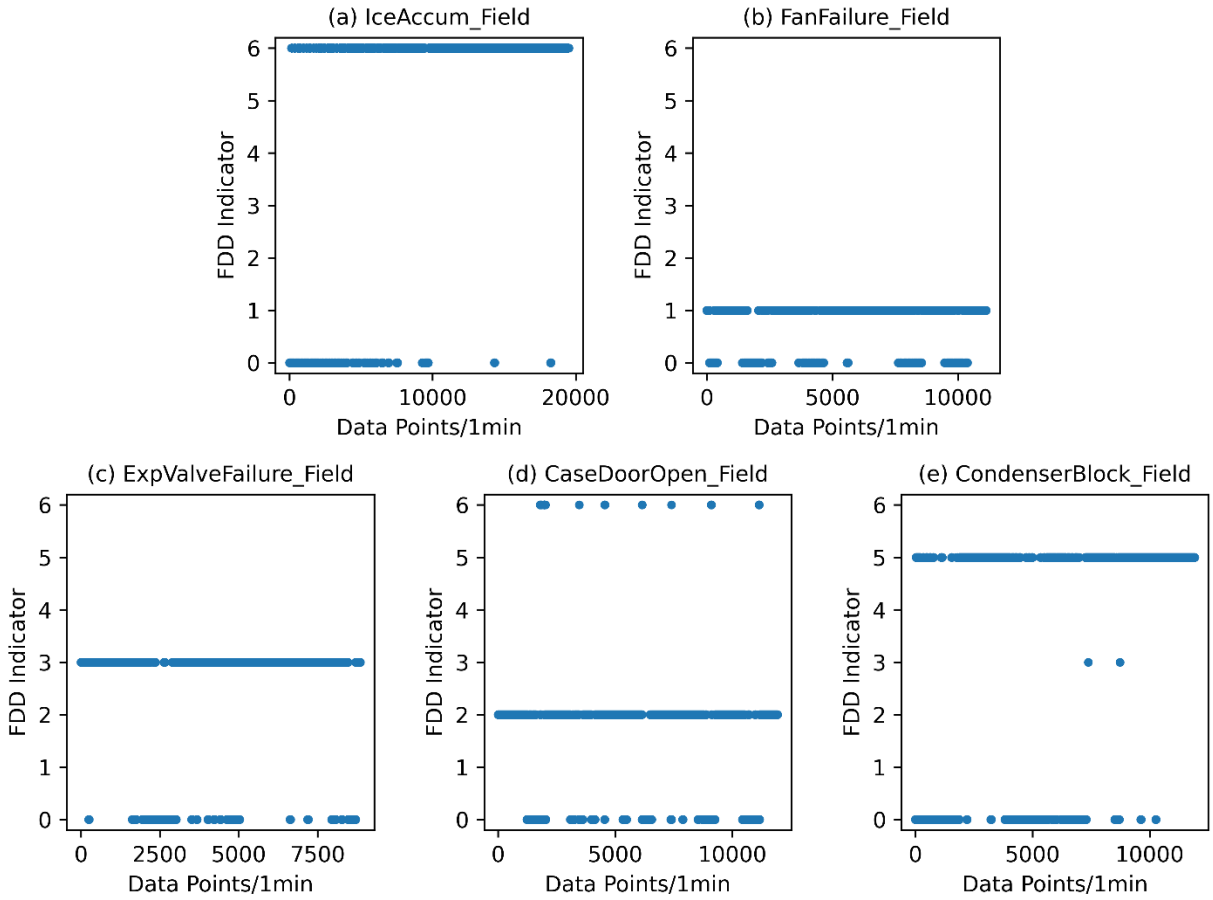

Figure 22. FDD for the fault measurement data.

Figure 22 shows that more than 90% of data points are detected successfully for the fault measurements. The percentage for each of the five fault detections are 91.5% for ice accumulation on the evaporator coil, 90.1% for evaporator fan partial failure, 90.6% for expansion valve failure, 90.01% for display door open, and 91.1% for condenser blockage. These values indicate the robustness of the proposed FDD algorithm. For three faults (ice accumulation on the evaporator coil, evaporator fan partial failure, expansion valve failure), the FDD indicates a correct index with a few 0 points.

However, for the display door open fault ((d) in Figure 22), there are a few FDD index values of 6, which is the ice accumulation on the evaporator coil fault. For the condenser blockage fault ((e) in Figure 22), there are some FDD index values of 3, which is the expansion valve failure fault. This indicates two improvements for future work: more measurement points need to be added, and filtering for noise needs

to be added. Actual system operations are dynamic. There are a couple noise types in the system, such as measurement noise, system noise, and other disturbances. Those noises affect fault detection. Especially for small faults, the differences between fault and normal operations are small. The noise might lead to misleading fault detection results.

Above fault detections only applicable for single fault situations. For concurrent faults, or more than two faults, the FDD algorithm needs further improvement in future studies. This FDD is currently for offline fault detection, and online deployable FDD algorithms will be developed for real refrigeration systems.

4.5.3 FDD in the Simulation Environment

Figure 23 demonstrates the FDD results for the simulated data for the five faults investigated. The FDD value of 0 denotes the fault-free condition. The FDD value of greater than 0 indicates the fault types as proposed from the FDD algorithm. Based on simulation data, the FDD shows 100% detection of faults.

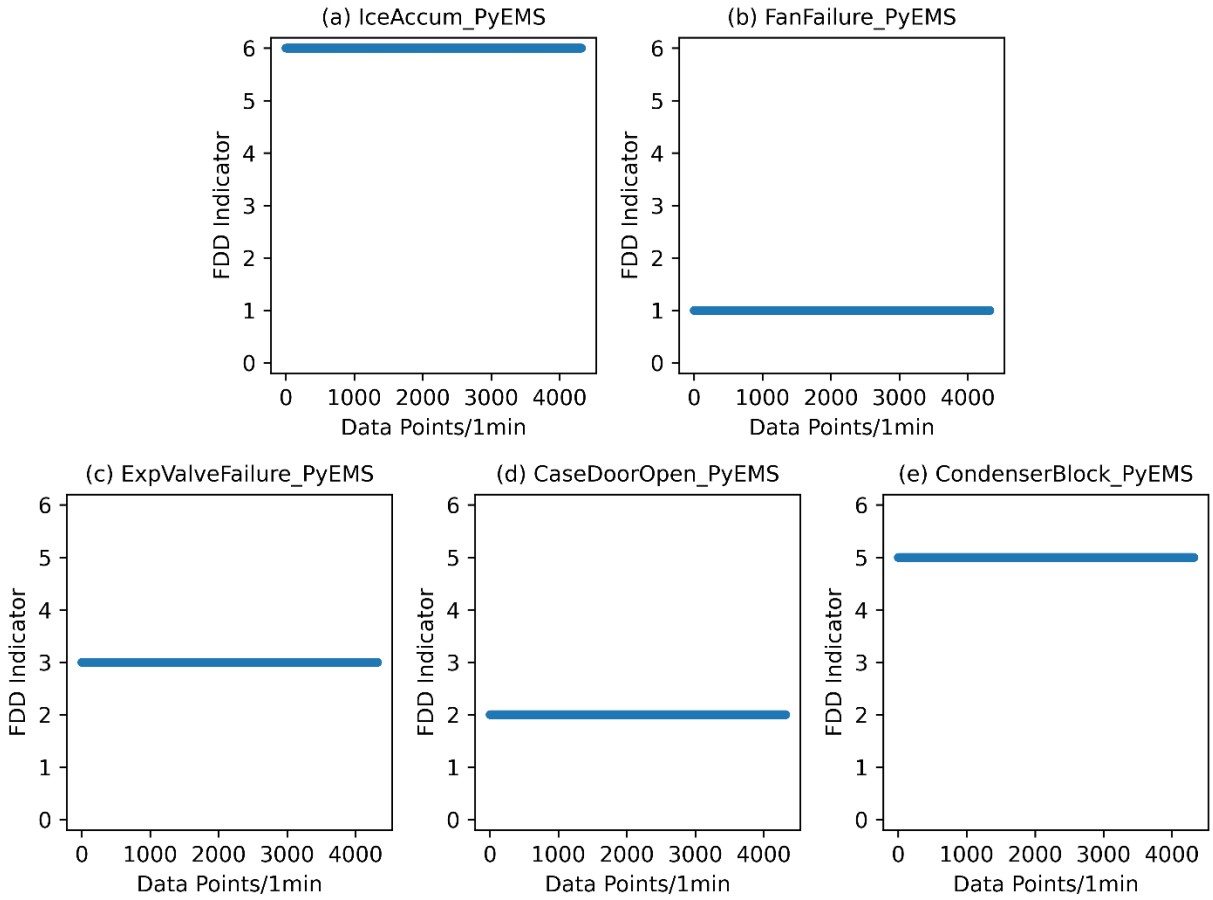

Figure 23. FDD for the fault modeling results.

5. CONCLUSIONS

This study demonstrates results from the fault models developed and calibrated for supermarket transcritical CO_2 refrigeration systems. The study involved three steps: (1) five fault models regarding the power consumption and SAT were proposed for low- and high-temperature compressors; (2) the fault models were calibrated with field tests, and the modeling accuracies were in good agreement with the measurement data set based on the RMSE; and (3) FDD was performed based on the developed fault models, which have greater than 90% fault detection accuracy. Overall, the fault models function as expected.

Multiple items will be explored in future work. They are summarized as follows:

- The current measurement data set does not measure cooling capacity, which is an important consideration for fault models and could be explored in future studies.
- The current set of fault models is at the system level—not enough fault data were developed for the component level. Adding component-based fault models for components such as the compressor, condenser, and expansion valve is extremely important.
- The CO_2 refrigeration system models in EnergyPlus are ideal models with limited input parameters. Developing high-fidelity dynamic refrigeration models is highly desirable. Accurate FDD also requires more dynamic models.
- Deploying the proposed fault models in the actual CO_2 refrigeration equipment is desirable for field studies to further evaluate fault detection accuracy.
- A challenge remains to detect multiple faults that occur concurrently.

6. REFERENCES

AHRI. 2012. “Standard for Performance Rating of Positive Displacement Carbon Dioxide Refrigerant Compressors and Compressor Units.” Air Conditioning, Heating, and Refrigeration Institute. https://www.ahrinet.org/App_Content/ahri/files/STANDARDS/ANSI/ANSI_AHRI_Standard_571_SI_2012.pdf.

Behfar, Alireza, and David Yuill. 2020. “Numerical Simulation of Fault Characteristics for Refrigeration Systems with Liquid Line Receivers.” *International Journal of Refrigeration* 119: 11–23.

Calm, James M. 2008. “The next Generation of Refrigerants–Historical Review, Considerations, and Outlook.” *International Journal of Refrigeration* 31 (7): 1123–33.

Cheung, Howard, and James E. Braun. 2015. “Development of Fault Models for Hybrid Fault Detection and Diagnostics Algorithm.”

Howard Cheung, James Braun. 2016. “Empirical Modeling of the Impacts of Faults on Water-Cooled Chiller Power Consumption for Use in Building Simulation Programs.” *Applied Thermal Engineering* 99: 756–64.

Drgoňa, Ján, Javier Arroyo, Iago Cupeiro Figueroa, David Blum, Krzysztof Arendt, Donghun Kim, Enric Perarnau Ollé, Juraj Oravec, Michael Wetter, and Draguna L. Vrabie. 2020. “All You Need to Know about Model Predictive Control for Buildings.” *Annual Reviews in Control*.

Ersoy, H. Kursad, and Nagihan Bilir Sag. 2014. “Preliminary Experimental Results on the R134a Refrigeration System Using a Two-Phase Ejector as an Expander.” *International Journal of Refrigeration* 43: 97–110.

Fricke, Brian A., and Vishaldeep Sharma. 2016. “High Efficiency, Low Emission Refrigeration System.” ORNL/TM-2016/363. ORNL/TM-2016/363, Oak Ridge National Laboratory (ORNL).

Ge, Y. T., and S. A. Tassou. 2011. “Thermodynamic Analysis of Transcritical CO2 Booster Refrigeration Systems in Supermarket.” *Energy Conversion and Management* 52 (4): 1868–75.

Hafner, Armin, Sven Försterling, and Krzysztof Banasiak. 2014. “Multi-Ejector Concept for R-744 Supermarket Refrigeration.” *International Journal of Refrigeration* 43: 1–13.

Halimic, E., D. Ross, B. Agnew, A. Anderson, and I. Potts. 2003. “A Comparison of the Operating Performance of Alternative Refrigerants.” *Applied Thermal Engineering* 23 (12): 1441–51.

Hovgaard, Tobias Gybel, Lars F. S. Larsen, Kristian Edlund, and John Bagterp Jørgensen. 2012. “Model Predictive Control Technologies for Efficient and Flexible Power Consumption in Refrigeration Systems.” *Energy*, Integration and Energy System Engineering, European Symposium on Computer-Aided Process Engineering 2011, 44 (1): 105–16. https://doi.org/10.1016/j.energy.2011.12.007.

Hwang, Yunho, Dae-Hyun Jin, and Reinhard Radermacher. 2007. “Comparison of R-290 and Two HFC Blends for Walk-in Refrigeration Systems.” *International Journal of Refrigeration* 30 (4): 633–41.

ICF Consulting. 2005. “Revised Draft Analysis of U.S. Commercial Supermarket Refrigeration Systems.”

Kim, Man-Hoe, Jostein Pettersen, and Clark W. Bullard. 2004. “Fundamental Process and System Design Issues in CO2 Vapor Compression Systems.” *Progress in Energy and Combustion Science* 30 (2): 119–74.

Koeln, Justin P., and Andrew G. Alleyne. 2014. “Optimal Subcooling in Vapor Compression Systems via Extremum Seeking Control: Theory and Experiments.” *International Journal of Refrigeration* 43: 14–25.

Li, Pengfei, Yaoyu Li, John E. Seem, Hongtao Qiao, Xiao Li, and Jon Winkler. 2014. “Recent Advances in Dynamic Modeling of HVAC Equipment. Part 2: Modelica-Based Modeling.” *HVAC&R Research* 20 (1): 150–61.

Li, Pengfei, Hongtao Qiao, Yaoyu Li, John E. Seem, Jon Winkler, and Xiao Li. 2014. “Recent Advances in Dynamic Modeling of HVAC Equipment. Part 1: Equipment Modeling.” *HVAC&R Research* 20 (1): 136–49.

Li, Wenhua, Shenglan Xuan, and Jian Sun. 2012. “Entropy Generation Analysis of Fan-Supplied Gas Cooler within the Framework of Two-Stage CO2 Transcritical Refrigeration Cycle.” *Energy Conversion and Management* 62: 93–101.
Li, Yanfei, and Zheng O’Neill. 2018. “A Critical Review of Fault Modeling of HVAC Systems in Buildings.” In *Building Simulation*, 11:953–75. Springer.
Li, Yanfei, Zheng O’Neill, Liang Zhang, Jianli Chen, Piljae Im, and Jason DeGraw. 2021. “Grey-Box Modeling and Application for Building Energy Simulations-A Critical Review.” *Renewable and Sustainable Energy Reviews* 146: 111174.
Mota-Babiloni, Adrián, Joaquín Navarro-Esbrí, Ángel Barragán-Cervera, Francisco Molés, Bernardo Peris, and Gumersindo Verdú. 2015. “Commercial Refrigeration–an Overview of Current Status.” *International Journal of Refrigeration* 57: 186–96.
Qian, Defeng, Yanfei Li, Fuxin Niu, and Zheng O’Neill. 2019. “Nationwide Savings Analysis of Energy Conservation Measures in Buildings.” *Energy Conversion and Management* 188: 1–18.
Ricker, N. Lawrence. 2010. “Predictive Hybrid Control of the Supermarket Refrigeration Benchmark Process.” *Control Engineering Practice* 18 (6): 608–17.
Sarkar, Jahar. 2012. “Ejector Enhanced Vapor Compression Refrigeration and Heat Pump Systems—A Review.” *Renewable and Sustainable Energy Reviews* 16 (9): 6647–59.
Sharma, Vishaldeep, Brian Fricke, and Pradeep Bansal. 2014. “Comparative Analysis of Various CO2 Configurations in Supermarket Refrigeration Systems.” *International Journal of Refrigeration* 46: 86–99.
Silva, Alessandro da, Enio Pedone Bandarra Filho, and Arthur Heleno Pontes Antunes. 2012. “Comparison of a R744 Cascade Refrigeration System with R404A and R22 Conventional Systems for Supermarkets.” *Applied Thermal Engineering* 41: 30–35.
Sofos, Marina, Jared Langevin, Michael Deru, Erika Gupta, Kyle S. Benne, David Blum, Ted Bohn, Robert Fares, Nick Fernandez, and Glenn Fink. 2020. “Innovations in Sensors and Controls for Building Energy Management: Research and Development Opportunities Report for Emerging Technologies.” National Renewable Energy Lab.(NREL), Golden, CO (United States).
Sun, Jian. 2019. Power management for co2 transportation refrigeration system. United States US20190041111A1, filed February 1, 2017, and issued February 7, 2019. https://patents.google.com/patent/US20190041111A1/en.
Sun, Jian, Hans-Joachim Huff, Aryn Shapiro, Gilbert B. Hofsdal, Minfei Gan, and Wenhua Li. 2014. Termperature Control Logic For Refrigeration System. United States US20140151015A1, filed July 25, 2012, and issued June 5, 2014. https://patents.google.com/patent/US20140151015A1/en.
Sun, Jian, Piljae Im, Yeonjin Bae, Jeff Munk, Teja Kuruganti, and Brain Fricke. 2021a. “Fault Detection of Low Global Warming Potential Refrigerant Supermarket Refrigeration System: Experimental Investigation.” *Case Studies in Thermal Engineering* 26: 101–200.
Sun, Jian, Piljae Im, Yeonjin Bae, Jeff Munk, Teja Kuruganti, and Brian Fricke. 2021b. “Dataset of Low Global Warming Potential Refrigerant Refrigeration System for Fault Detection and Diagnostics.” *Scientific Data* 8 (1): 1–10.
Sun, Jian, Teja Kuruganti, Jeff Munk, Jin Dong, and Borui Cui. 2021. “Low Global Warming Potential (GWP) Refrigerant Supermarket Refrigeration System Modeling and Its Application.” *International Journal of Refrigeration* 126: 195–209.
Sun, Jian, and Lucy Yi Liu. 2019. Transcritical refrigerant vapor compression system high side pressure control. United States US10451325B2, filed August 20, 2013, and issued October 22, 2019. https://patents.google.com/patent/US10451325B2/en.
Sun, Jian, Mark J. Perkovich, Mary D. Saroka, and Jason R. Kondrk. 2018. Transport refrigeration system and method of operating. United States US20180304724A1, filed October 21, 2016, and issued October 25, 2018. https://patents.google.com/patent/US20180304724A1/en.
“Supermarket Facts.” 2021. August 24, 2021. https://www.fmi.org/our-research/supermarket-facts.
Venkatarathnam, G., and S. Srinivasa Murthy. 2012. “Refrigerants for Vapour Compression Refrigeration Systems.” *Resonance* 17 (2): 139–62.

Liang Yang, Chun-Lu Zhang. 2011. “On Subcooler Design for Integrated Two-Temperature Supermarket Refrigeration System.” *Energy and Buildings* 43 (1): 224–31.
Zhang, Liang, Jin Wen, Yanfei Li, Jianli Chen, Yunyang Ye, Yangyang Fu, and William Livingood. 2021. “A Review of Machine Learning in Building Load Prediction.” *Applied Energy* 285: 116452.